Sensor and Simulation Notes

Note 210

July 1975

Sweep Frequency Surface Field Measurements

Valdis V. Liepa
The University of Michigan
Ann Arbor, Michigan 48105

Abstract

The research described in this report is primarily experimental
and deals with the development of surface current and charge measure-
ment techniques for use on scale model aircraft. The report describes
a sweep measurement technique where measurements are made by
sweeping a frequency with the sensor fixed and positioned in turn at
selected measurement points of interest. Design and performance data
of a number of current and charge sensors are presented, including the
diode sensors that use high resistance telemetry leads for reduced
interaction with the model and the incident field. Results of a current
loop probe calibration study, for cases when fields are measured along
elements of small radii of curvature, are presented.

Measured data are presented for 747 model aircraft and models of
various degrees of similarity to the 747 shape to demonstrate the feasi-
bility of using a "rough model" in the surface current and charge mea-
surement program. Current measurements are also presented for the
so-called wire grid model used by the Air Force in the computation of
fields on the B-1 aircraft. Amplitude and phase data cover 1.5 to
16.5 MHz full-scale frequency range and explicitly show the basic reso-
nances of the structure.

76-047

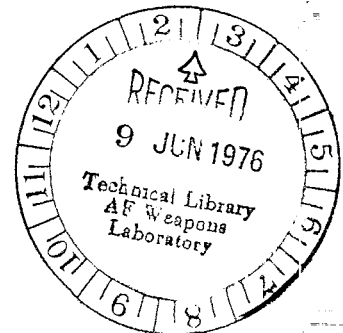Sensor and Simulation Notes

Note 210

July 1975

Sweep Frequency Surface Field Measurements

Valdis V. Liepa
The University of Michigan
Ann Arbor, Michigan 48105

Abstract

The research described in this report is primarily experimental
and deals with the development of surface current and charge measure-
ment techniques for use on scale model aircraft. The report describes
a sweep measurement technique where measurements are made by
sweeping a frequency with the sensor fixed and positioned in turn at
selected measurement points of interest. Design and performance data
of a number of current and charge sensors are presented, including the
diode sensors that use high resistance telemetry leads for reduced
interaction with the model and the incident field. Results of a current
loop probe calibration study, for cases when fields are measured along
elements of small radii of curvature, are presented.

Measured data are presented for 747 model aircraft and models of
various degrees of similarity to the 747 shape to demonstrate the feasi-
bility of using a "rough model" in the surface current and charge mea-
surement program. Current measurements are also presented for the
so-called wire grid model used by the Air Force in the computation of
fields on the B-1 aircraft. Amplitude and phase data cover 1.5 to
16.5 MHz full-scale frequency range and explicitly show the basic reso-
nances of the structure.

76-047

PREFACE

The author is grateful to Fred P. Rhine of the Radiation Laboratory for his assistance in performing the measurements and to Professors R. E. Hiatt and T. B. A. Senior for helpful suggestions and discussions. The assistance of AFWL personnel in the course of this study is also greatly appreciated.

CONTENTS

ILLUSTRATIONS

Illustrations, continued

SECTION I

INTRODUCTION

The objectives of this research were to:

1. Develop charge measuring techniques and develop techniques for amplitude and phase measurements of current and charge in the sweep frequency mode.

2. Provide experimental data to verify computer codes for wire models.

3. Devise error-correction techniques for measurements near edges.

4. Modify the equipment and/or the techniques as needed to allow reliable measurements to be made at lower frequencies.

5. Determine whether or not it is feasible to use crude models in low frequency measurements.

6. Perform sample measurements to demonstrate the capability of the facility.

During the course of the study, all of the stated requirements have been satisfactorily completed.

The work performed included the development of monopole and disc type charge probes, the development of charge probes using high resistance leads for carrying the detected signal to the receiver, thus avoiding the need for using metallic leads, and the design and construction of the electronics needed for use with the diode type charge probes.

A major innovation was the development of techniques for using a swept frequency system for obtaining and recording data as a function of frequency. A swept frequency signal generator was used as a source and the Hewlett-Packard network analyzer was used as a tracking receiver and it provided both amplitude and phase information. As is shown by the data included later in the report, these techniques provide excellent results. The effort required is less than that needed when using the fixed frequency method (ref. 1). It should be noted, however, even

---

1. E. F. Knott, "Surface Field Measurements," Interaction Application Memos, Memo 5, Air Force Weapons Laboratory, Kirtland AFB, NM, September 1974.

though the swept frequency method provides continuous (raw) data, the data must be reduced or normalized with respect to the incident field. This reduction is done manually, and this accounts for the discrete data points for amplitude and phase data vs. frequency as presented in this report.

In the task where the feasibility of using crude models was examined, current data were measured as a function of frequency on scale model Boeing 747 aircraft of various degrees of perfection. Three models were used in this study. The swept frequency range covered included the critical resonant frequencies of the aircraft. This study is discussed in Section III.

Measurements were made to provide data to compare with those obtained with computer codes for wire models. Use was made of the so-called wire grid model employed by Taylor et al. (ref. 2) in their computation of current on the B-1. For the wings in the forward and swept positions, five different measurements were made and data are presented for the 1.5 to 16.5 MHz full-scale frequency range. Of particular interest are the data measured on the top and bottom of the fuselage for the case of symmetric excitation with illumination from above. Since these data represent the current for the illuminated and shadow side of the fuselage, they should provide valuable information for determining the validity of various thick wire model computer codes, especially when they are used at frequencies beyond the first resonance peak. The results are discussed in Section IV.

In summary, the experimental facility is discussed in Section II; Section III contains a description of the various experimental studies. The results of the sample measurements are presented in Section IV and Section V contains a summary of the research effort and present capabilities.

_____

2. C.D. Taylor, K.T. Chen, and T.T. Crow, "An Improvement on Wire Modeling for EMP Interaction with Aircraft," EMP Interaction Notes, Note 241, Air Force Weapons Laboratory, Kirtland AFB, NM, October 1974.

SECTION II

EXPERIMENTAL FACILITY

1. CHAMBER

The surface field measurement facility has been described in detail in IAM No. 5 by Knott (ref. 1). Briefly, the facility consists of a 40-ft long tapered design anechoic chamber with the transmitting antenna placed at the apex of the tapered section and the receiving or working area, which is rectangular in cross section and is 11 ft deep, 10 ft high and 12 ft wide, at the other end. A probe positioning mechanism that provides both cylindrical and cartesian direction of motion is mounted above the ceiling. A balsa wood tower extends downward, supporting either charge or current probe. The model on which the surface fields are measured is supported by a styrofoam column placed on the floor underneath the probe positioning equipment.

Up until the present program, the surface field measurements were made at single fixed frequencies by moving a probe along a prescribed trajectory on the surface of the body to determine the surface field amplitude at selected points on the trajectory. At each point the operator would go into the chamber, position the probe, and then leave the chamber to obtain a measurement of the field amplitude at that point. When another frequency was required, the frequency of the illuminating cw field was changed appropriately and the procedure repeated. Thus, for numerous scans or frequencies, or sampling at closely spaced points, the operating was a very time-consuming one.

With the present need for surface data as a function of frequency, rather than of position along the surface of the body, the cw technique is very cumbersome and rather impractical. Consequently, a swept frequency scheme for measuring the fields was developed and, as the data presented in this report verify, the technique provides excellent data. Nevertheless, there are still areas where improvements can be made, and we would hope to incorporate these changes in future programs of this type.

2. EQUIPMENT

Figure 1 shows a block diagram of the chamber and the equipment used for sweep frequency measurements. It differs from the one used previously (ref. 1) primarily in instrumentation. For single frequency measurements, such as done by Knott, the basic instruments required were (1) tunable cw source, (2) microwave receiver, and (3) display indicator, such as a VSWR meter. For a sweep measurement facility, about three times as much equipment is required, and likewise, the cost for such equipment is also about three times as much as for the single-frequency equipment.

The basic ingredients of a sweep measurement system are a sweep generator and a tracking receiver (HP 8410S network analyzer). These are supplemented by the additional components shown in Fig. 1. On the transmitter end, a signal from the sweep generator (10 mw, nominal) is first amplified by a traveling wave amplifier (TWT) to about 1 watt. This provides an increase of signal-to-noise ratio at the receiver end. (This amplifier is optional, and probably would not be used when a preamplifier is used between the sensor and the network analyzer.) After the TWT, the signal goes through a 20dB coupler, an isolator, and then to the transmitting antenna. The coupler provides the reference signal for the receiver and the isolator reduces antenna reflections which may become large as a result of the extended frequency range.

On the receiving/recording side a signal (proportional to the current, or charge density) is picked up by a sensor and amplified before going into the signal port of the network analyzer. At present we do not have such an amplifier, and to maintain a sufficiently high signal-to-noise ratio, a TWT amplifier is used in the transmit side to boost the transmitted signal. To obtain a relatively flat phase difference between the reference and signal channels, the two signal paths should be of equal electric lengths. For gross adjustment of the electric lengths, coaxial cables are used, and for fine adjustment a line stretcher and a precision phase shifter are used.

When a measurement is taken, the amplitude and phase data are typically recorded by an X-Y recorder on 8.5 x 11 inch graph paper, with amplitude (dB) and
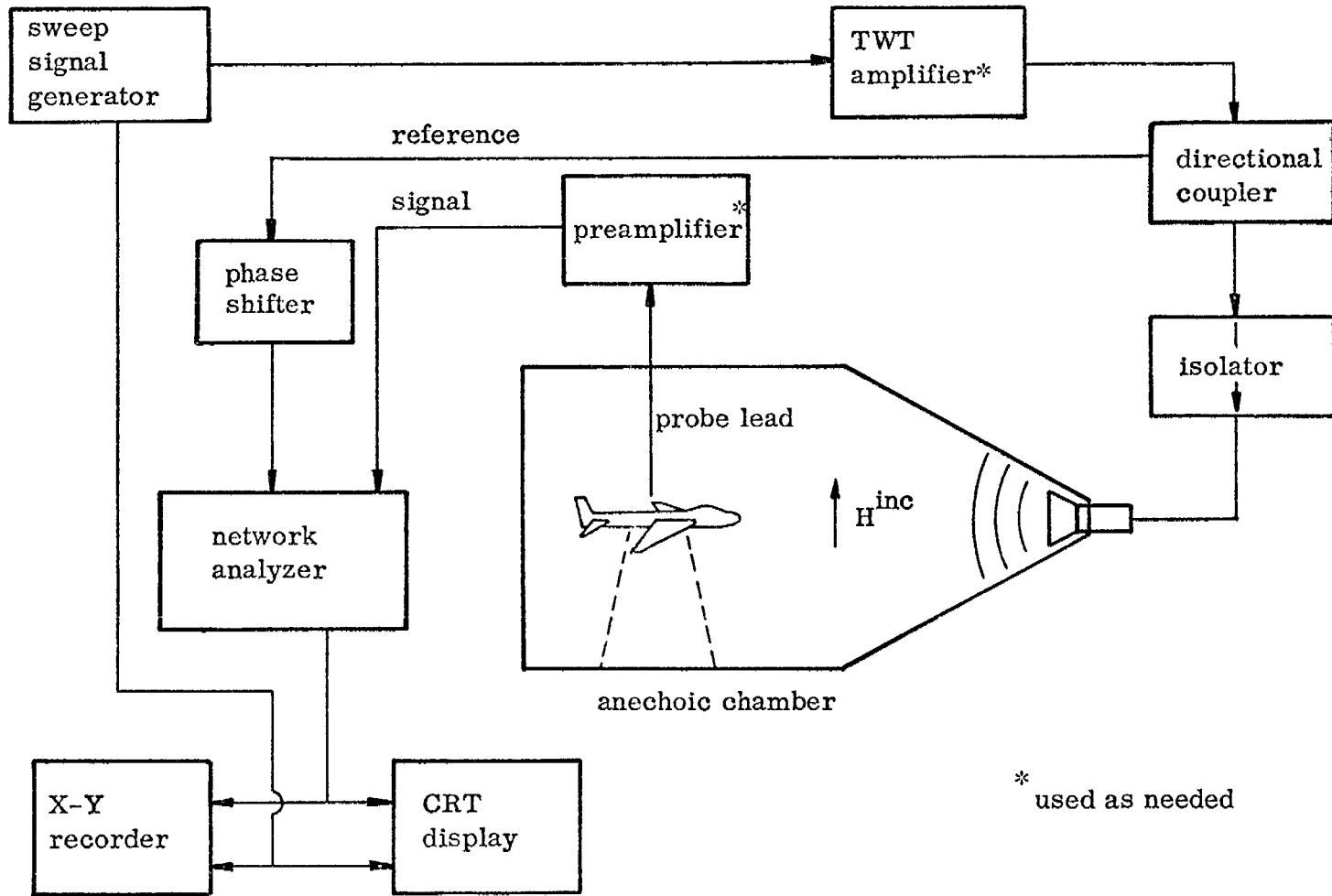
9

FIG. 1: Block diagram of surface field measurement facility.

phase (degrees) on the vertical scale and frequency on the horizontal scale. The CRT display is used for "tuning up" the system prior to recording. This includes adjusting the reflector of the TWT amplifier, tuning the antenna, setting the power output of the sweep generator, and adjusting the phase shifter. All adjustments are made to obtain a reasonably flat amplitude/frequency response over the frequency band.

To present a cursory view of the sweep measurement technique for a typical measurement procedure, the resultant raw data and the final reduced data are presented. In this example, the charge on the model (a 3.133-inch diameter sphere) is measured. In this case the charge probe is mounted (taped) on the model; the model is placed in the chamber and the phase and amplitude data are recorded on the X-Y plotter as the frequency is swept over the 1-2 GHz range. The same measurement is repeated, but this time with a 6-inch diameter reference sphere that will provide the calibration for the incident field. Care must be taken that the two models are placed at the same phase reference plane in the chamber, otherwise an offset in the phase data will result.

Figure 2 shows the raw amplitude and phase data of the normal electric field as measured at the shadow boundary of the 3.133-inch diameter sphere and recorded on the X-Y plotter. Note that even though various tuning adjustments were made prior to these measurements, both the amplitude and phase data exhibit numerous noise-like ripples over the band. These can be attributed, in part, to the transmitting antenna, reflections from the chamber walls and numerous mismatches in the cables, especially in the connectors. The wiggles can be decreased somewhat by adding small attenuator pads in critical places in the system, but these also attenuate the signal and thus may add "real" noise in the data.

Since it would be very difficult, if not impossible, to develop a measurement system such as ours in which the absolute incident field strength would be flat, say within 1 dB over a 2:1 frequency band, a calibration run is made to determine the incident field amplitude and phase over the frequency band of the test. This can be done either by measuring the incident field directly, or by measuring the field on a body for which the fields are known in relation to the incident field. Thus, a
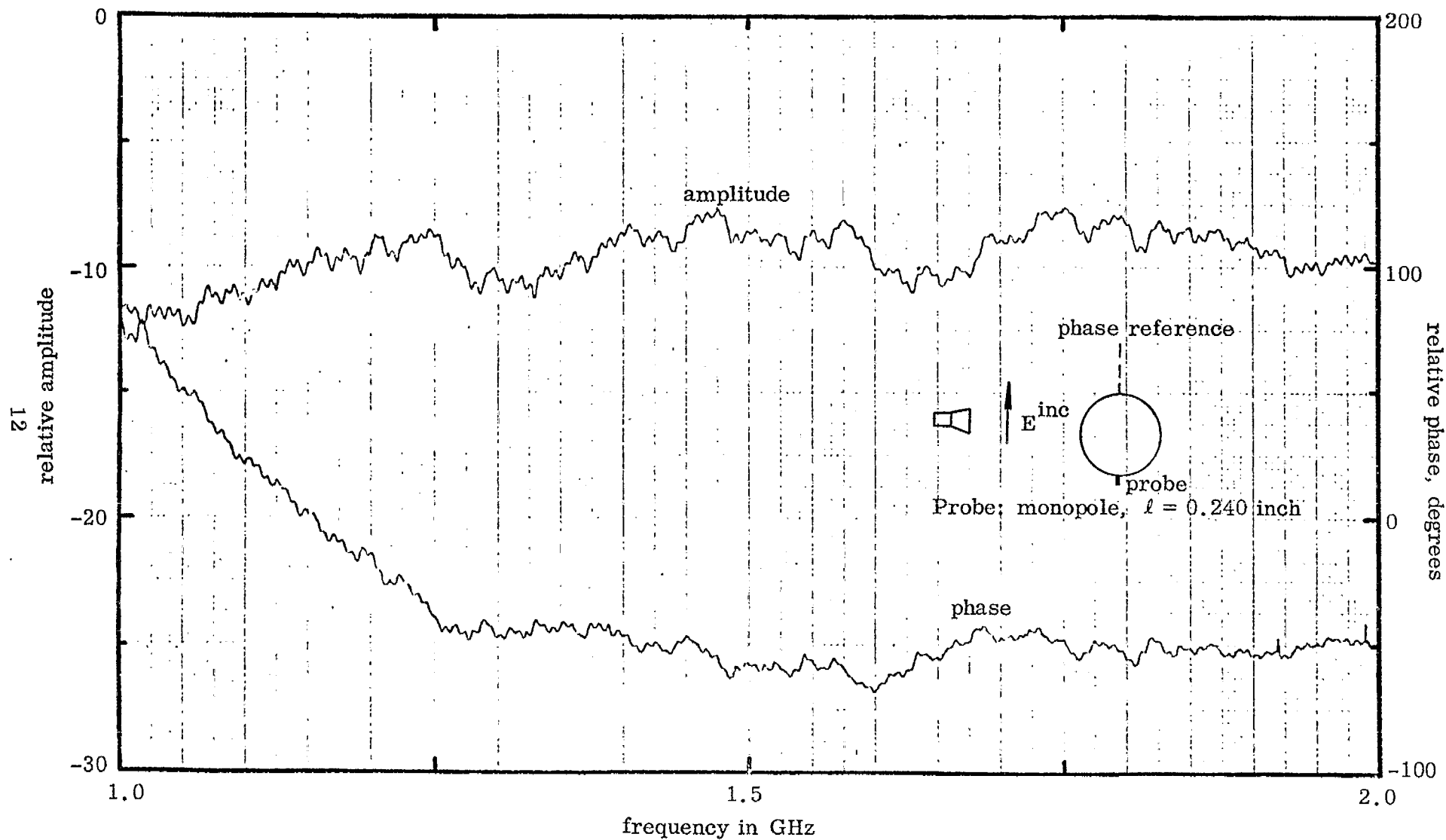
11

FIG. 2: Raw charge data for the 3.133-inch diameter sphere (test object) measured at shadow boundary.

measurement of amplitude and phase on a reference sphere can be easily translated to the corresponding incident field values using Mie series computations, for example. Also, in order to keep the experimental errors to a minimum, it is appropriate to use the same probe (i.e., sensor) to measure the surface field for the model as well as for the calibration of the incident field. Expecially when a sensor is of the surface mounted type, some type of surface must always be provided, and for this we have found a sphere to be an excellent choice.

The measurement of charge on a 6-inch diameter sphere for incident field determination is shown in Fig. 3. Comparison of Figs. 2 and 3 shows that the corresponding amplitude and phase curves are quite similar, with slowly varying separation between the corresponding amplitude and phase curves. Also, the same small wiggles appear on each of the curves, and since the difference between the corresponding curves is of concern, the presence of the wiggles makes reduction of the data more tedious, but not necessarily less accurate.

The results reduced from the raw data are presented in Fig. 4, and these are then compared with the theoretical values as computed from the Mie series for the same diameter sphere. Observe that the measured amplitude is about 1 dB low, except for the last point, which is about 3 dB high. This was caused by the loss of track by the network analyzer, as can be seen by the curve jump in the upper right hand corner of Fig. 3, and therefore such a point should not be considered in assessing the accuracy of the measurements.

The corresponding phase data of the sphere measurement is shown in the lower part of the same figure and there is, on the average, about a ± 5 degree difference between the experimental and theoretical data over the frequency band used. This phase deviation is probably indicative of what can be achieved in our measurements, and we expect no major phase errors as a result of faults in electrical equipment; our concern must be with the accuracy with which a model and the reference sphere can be positioned and aligned in the chamber with respect to the arbitrary reference plane. For example, a similar measurement was made on the opposite side of the sphere where the charge amplitude should be the same, but the phase should differ by 180 degrees. The measured amplitude was again in excellent

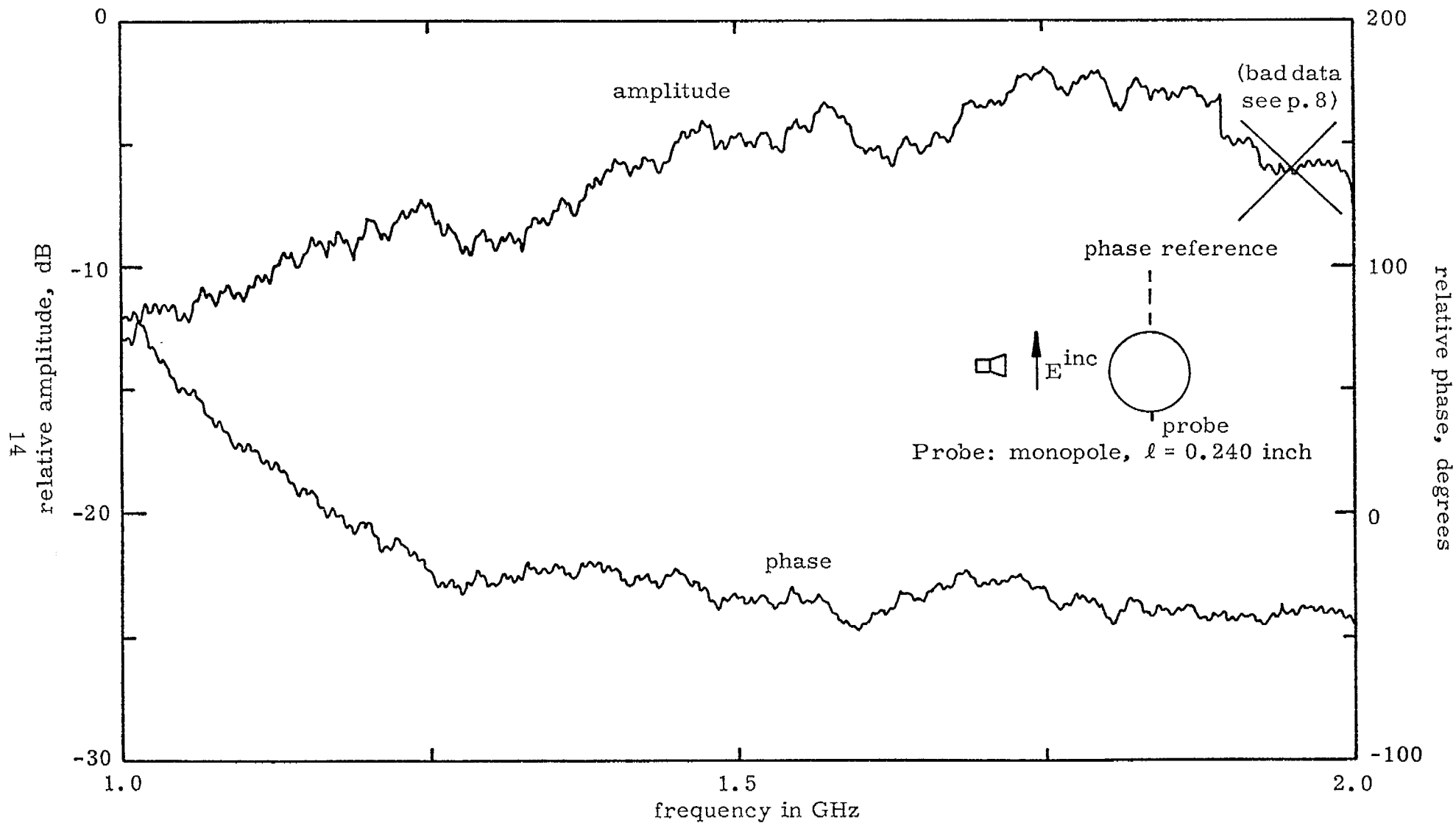FIG. 3: Raw charge data for the 6-inch diameter sphere (calibration sphere) measured at shadow boundary.
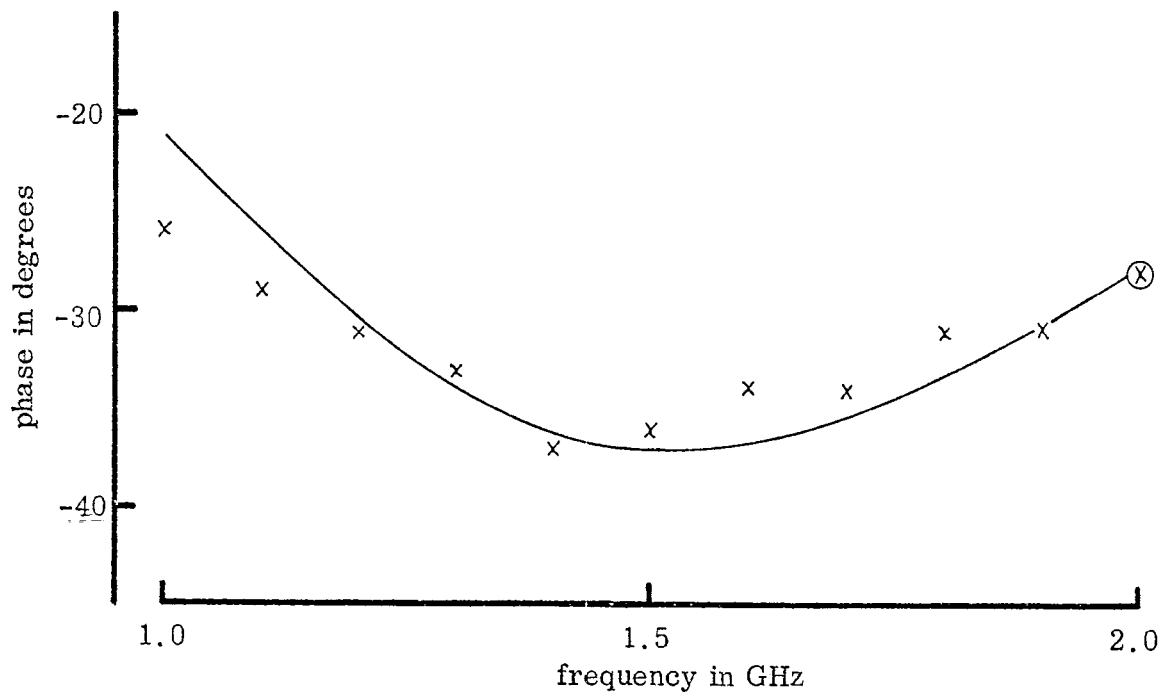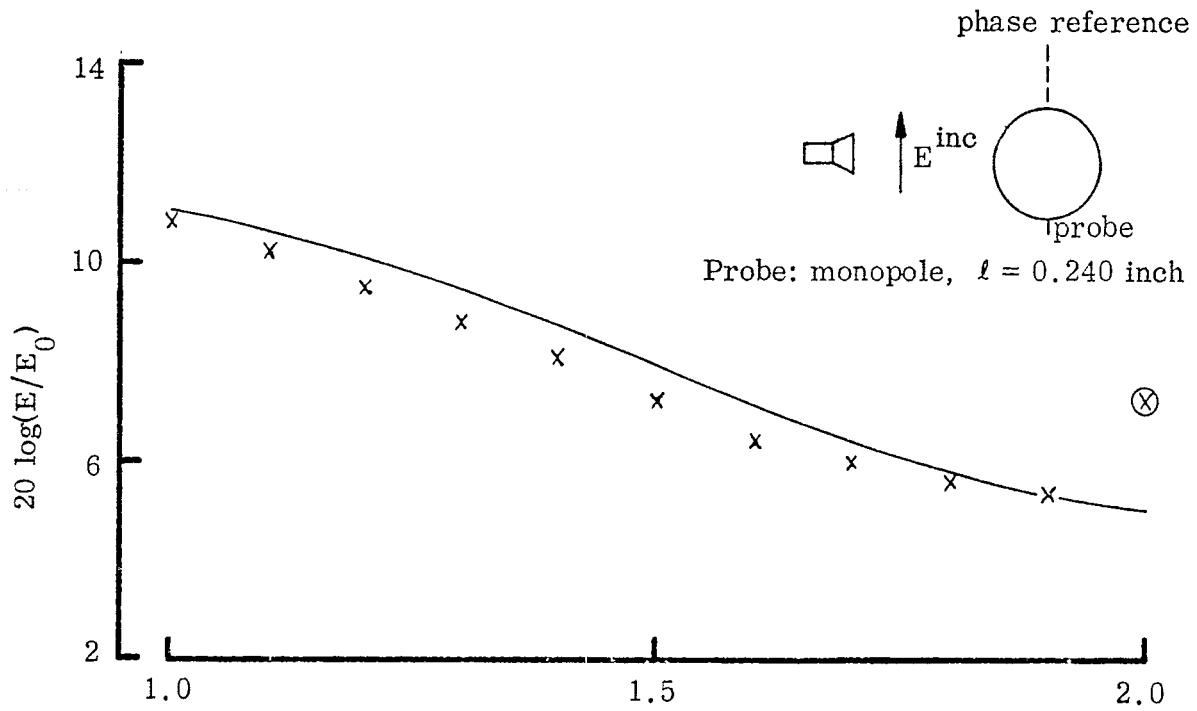
14

FIG. 4: Measured (✗✗✗) and theoretical (———) normal electric field at the shadow boundary of a 3.133-inch diameter sphere, $\theta = +90^\circ$.

agreement, but the phase was definitely offset by 5 degrees, apparently resulting from a 1/8-inch displacement of either the model or the reference sphere from the phase reference plane.

3. PROBES

An indispensable component in any current or charge measurement scheme is a probe or a sensor through which a surface current or charge is transferred into a measurable signal. In the past, most measurements at the facility have been surface current measurements and for these we have constructed and now have a dozen or so loop probes which are basically shielded unbalanced magnetic loops ranging in diameters from about 2 to 10 millimeters. Knott (ref. 1) has described the construction and performance of loop probes in the previous report; more detailed information about construction and characteristics of loop probes can be found elsewhere (ref. 3).

Using the measurement procedure described above for charge measurment, a surface current was measured at the specular point for the same model (a 3.133-inch sphere) using a loop probe (No. 221) and repeating the same measurement on a 6-inch diameter sphere for the incident field calibration. The reduced data is shown in Fig. 5, and a comparison with the theoretical values shows that the results here are very good. The amplitude agreement is within 0.5 dB and the phase difference is less than one degree. The high phase accuracy of this measurement can be attributed, for the most part, to the fact that it is easier to align the front of the sphere than the shadow boundary with respect to the reference plane. Also, the currents at the front of the sphere show less variation with position and frequency than does the charge at the shadow boundary, and consequently a small misalignment of the sensor near the front is not as critical as it would be at the shadow boundary.

To supplement the current measurement capability, some charge or D-dot probes were developed. Figure 6 shows the construction details of two such probes that are expected to be the "workhorses" in future measurement programs.

In the upper section the standard monopole is shown. It is made by attaching an OSSM connector (an Omni Spectra, Inc., product) to one end of a 2-foot long, 0.020 inch diameter, 50 ohm semi-rigid coaxial cable. The other end is then used for the probe. First, a piece of the outer conductor, about 0.3 in. long is removed, leaving

---

3. E. F. Knott, Study of Microwave Dosimetry, University of Michigan Radiation Laboratory Report 010531-1-F, July 1972.
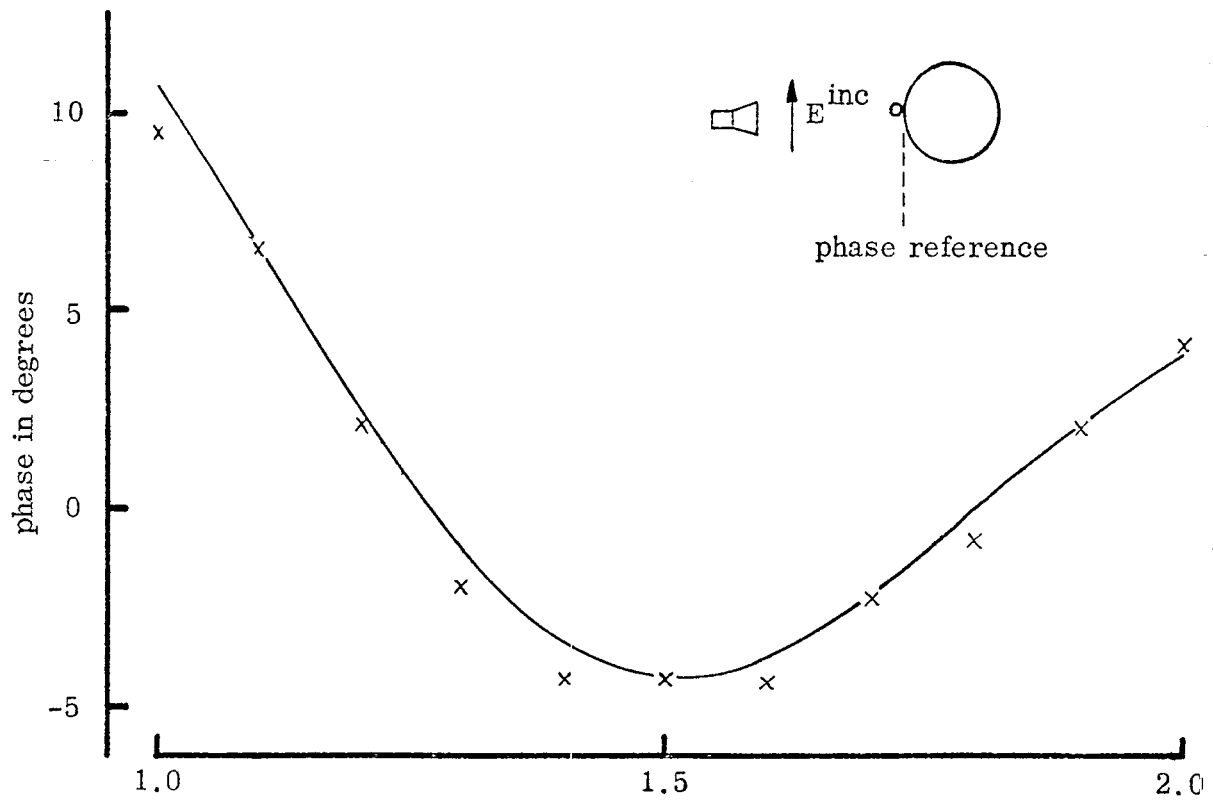
16
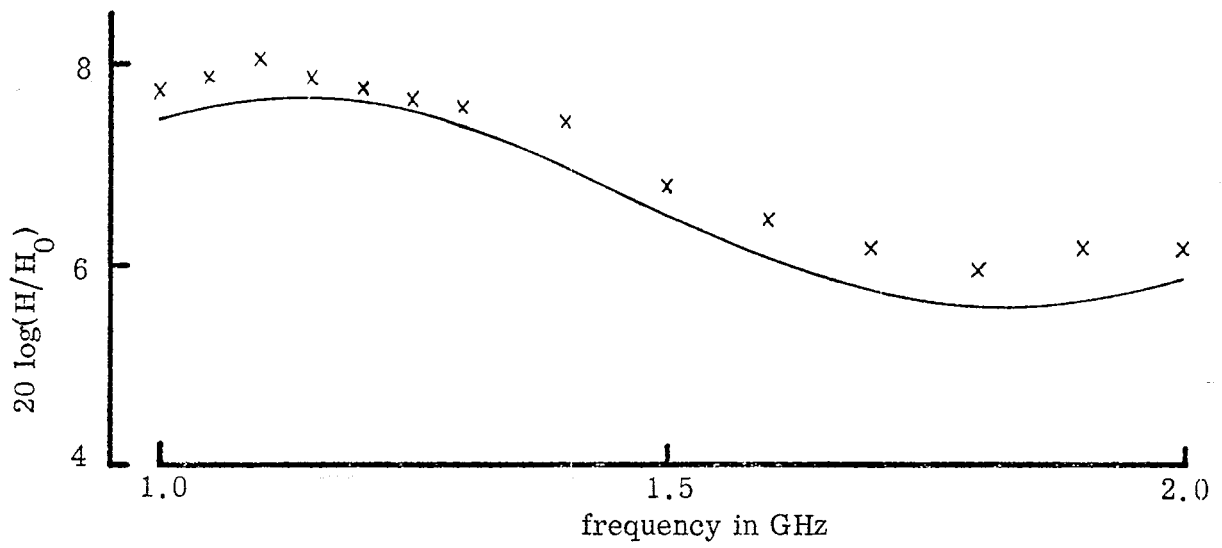
FIG. 5: Measured (x x x) and theoretical (——) current in front of a 3.133 inch diameter sphere

CENTER CONDUCTOR
AND DIELECTRIC; OUTER
SHIELD REMOVED

0.020" COAX
50 Ω

h

METAL DISC

0.5"

0.005" DIA.

(a) monopole

0.5"

CENTER CONDUCTOR

$\frac{5"}{32}$

DIELECTRIC

.032"

0.020" COAX
50 Ω

METAL DISK

0.005" DIA.
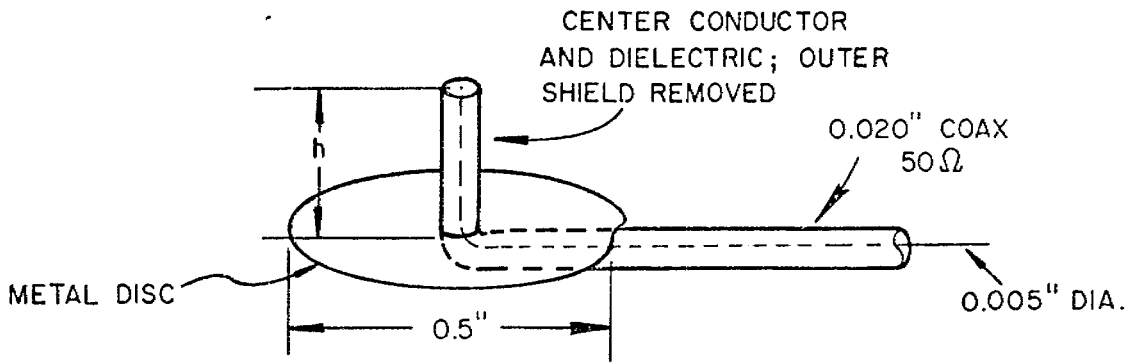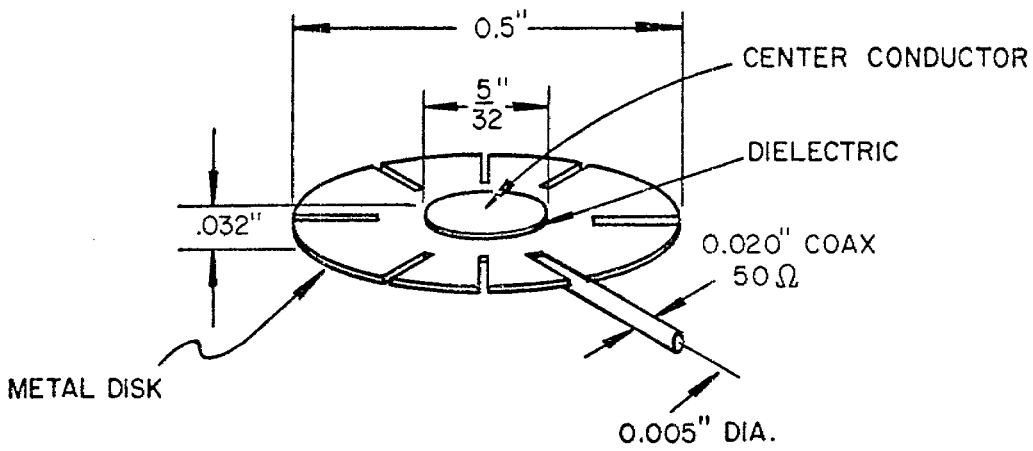
(b) disc

FIG. 6: Construction details of charge probes.

18

the insulation intact. The inner conductor forms a monopole which is then bent at right angles where the outer conductor ends. The monopole and coax are then taped with aluminum adhesive tape to the test object and to minimize the discontinuity near the base of the sensor, a piece of tape in which a small hole has been made is placed over the monopole.

When such a sensor is transferred from one object to another, or even from one place to another, the tape must be removed and retaped. During the process, the length or the height of the probe changes as much as 0.010 inch. Consequently, it is difficult to obtain the same length probe when it is transferred, but the resultant length of the mounted probe can be accurately measured to within ± 0.002 inch with a depth micrometer. Once the lengths are known, the data can be corrected. The study of the monopole length vs. signal received is presented in Section III, and there also the procedure is given for correcting for changes in the probe length.

The lower part of Fig. 6 indicates the construction details for the disc probe, patterned to some extent after the AFWL Model CFD-IA D-dot sensor, but smaller in diameter by a factor of 17. It consists of two discs, one 5/32 inch and the other 1/2 inch in diameter cut out of a G-10 printed circuit board material having a 0.015-inch fiberglass base and 0.001-inch copper on one side. The small disc is the active portion of the sensor and the larger disc provides a base through which the 0.020-inch ocaxial cable passes. The base has radial slots cut for easier flexing when mounting the sensor on a curved surface. When the sensor is mounted, the base disc is covered with tape to smooth the surface. Likewise, the coaxial cable is taped until it leaves the surface, usually on the opposite side of the body.

Although the charge data measured on a 3-inch sphere was presented previously (Fig. 4), for probe evaluation purposes it is essential that the measurements be made under similar conditions, preferably in sequence. Such measurements were made with the monopole and disc probes and the resulting data are presented in Figs. 7 and 8 respectively. In each case, the 6-in sphere was used as a reference. Note that the phase data are referenced at the front and not the center of the sphere as is customary. This shift was made to simplify the positioning or alignment of the model
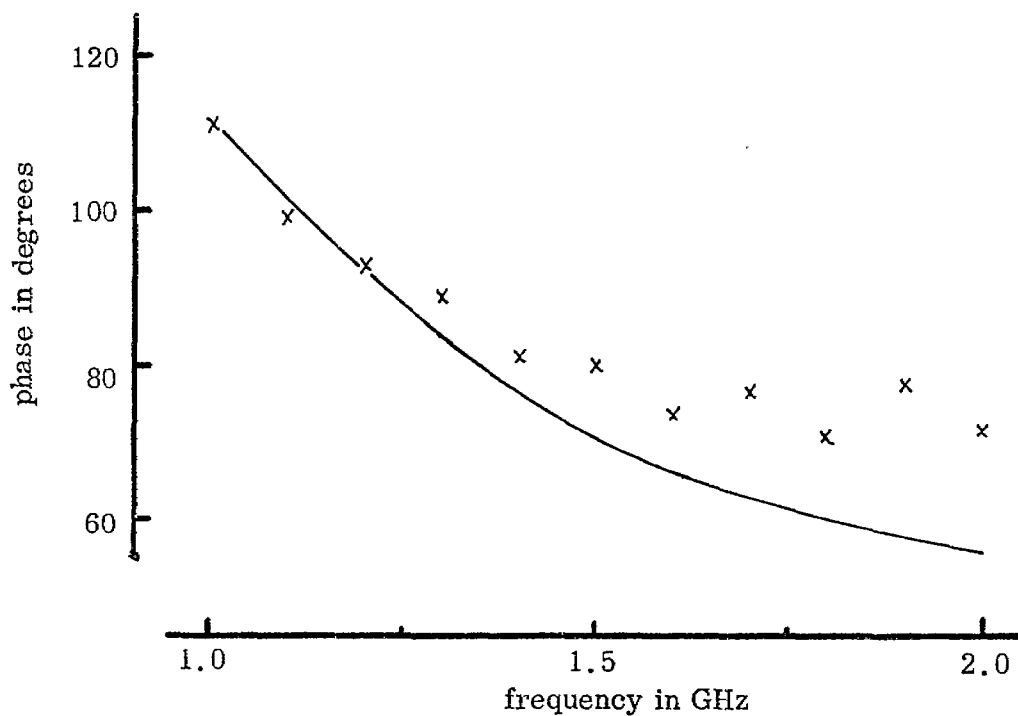
19
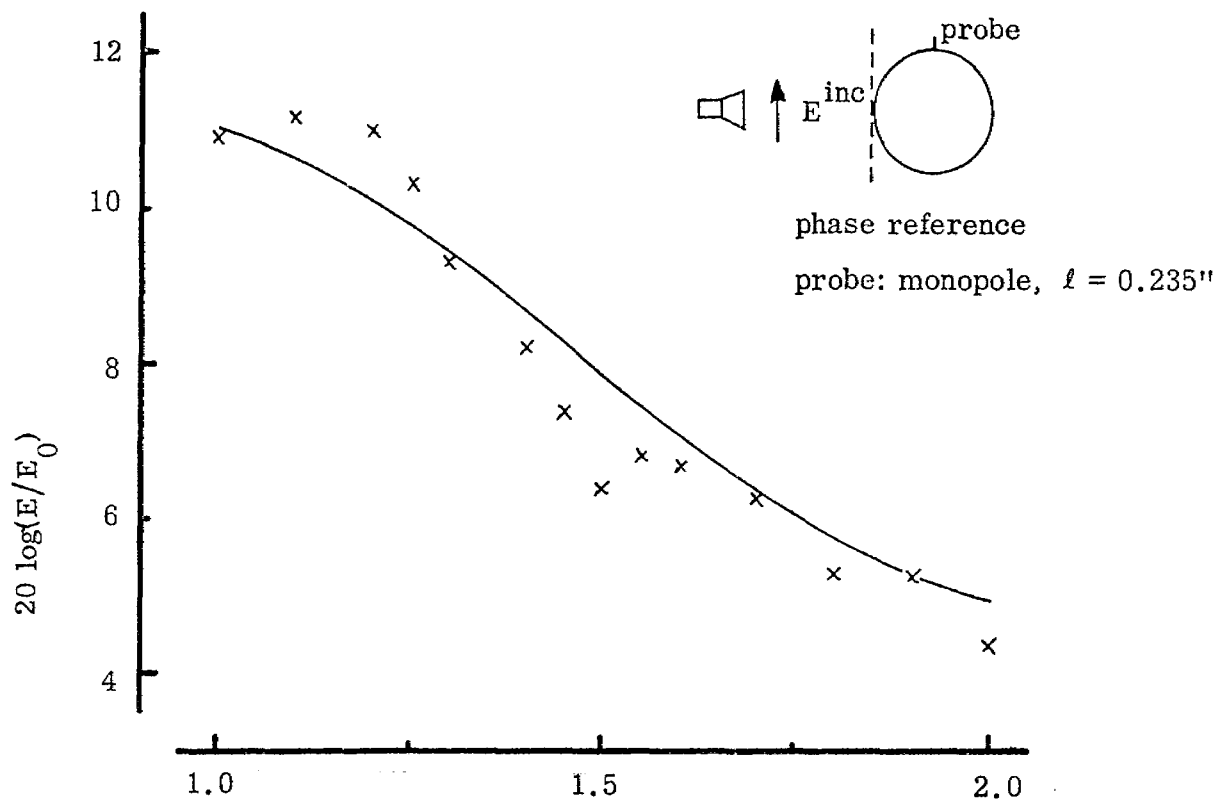
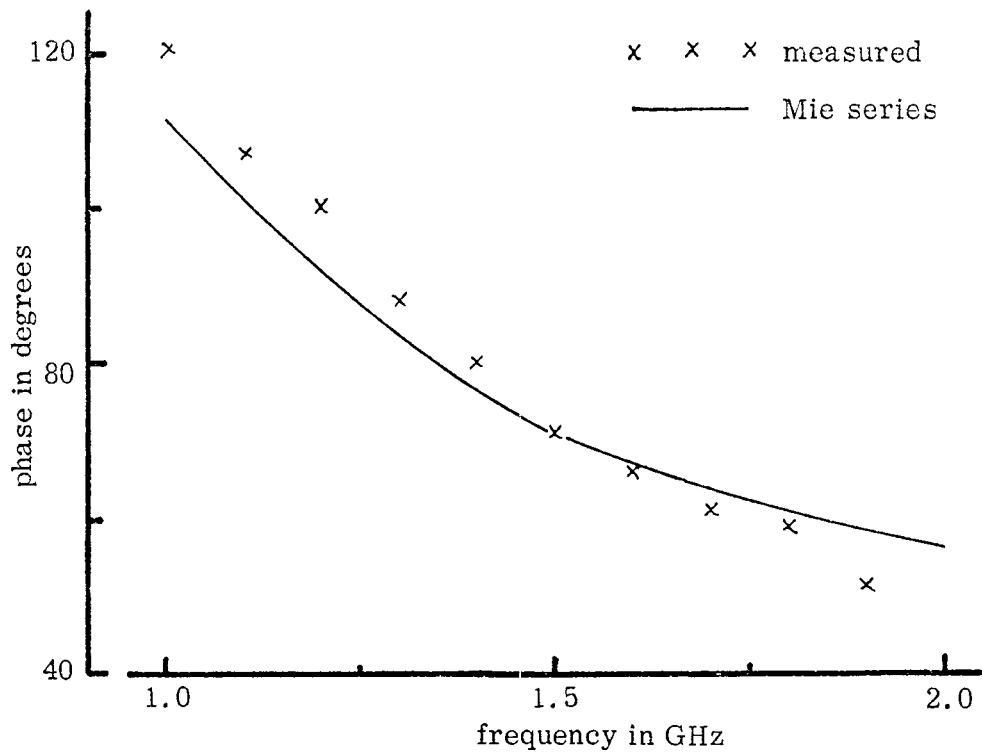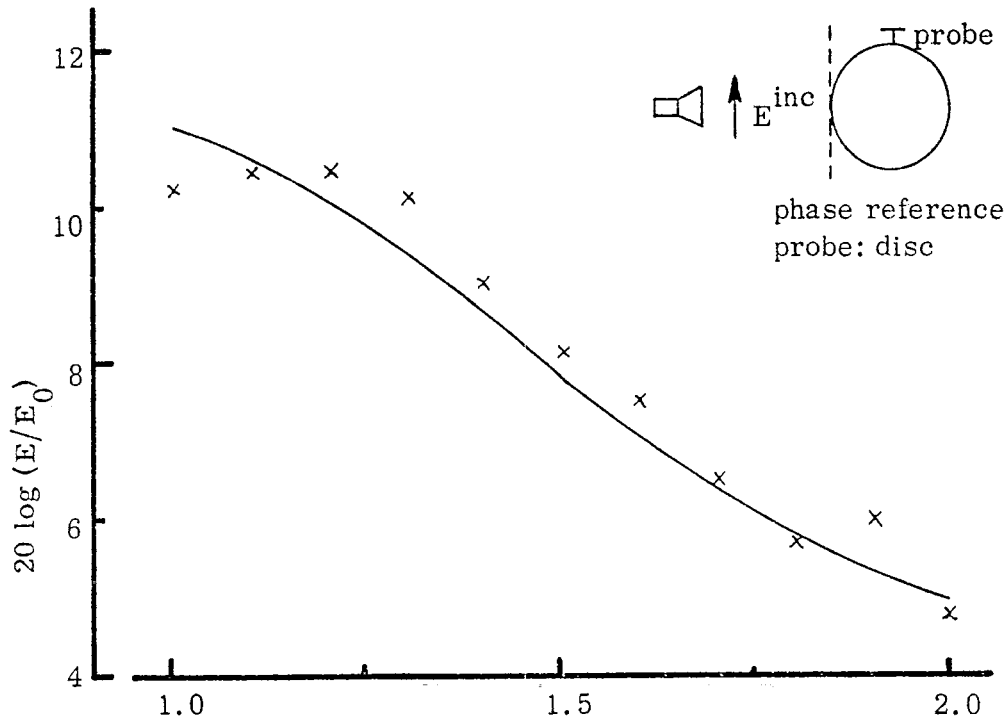FIG. 7: Charge measured with a monopole on a 3.133 inch diameter sphere.

FIG. 8: Charge measured with the disc probe on a 3.133 inch diameter
sphere.

(spheres) in the chamber. Physically this reference is a string stretched horizontally across the chamber perpendicular to the direction of propagation of the incident wave. Note that with the monopole the data measured here is not as accurate as that presented previously in Fig. 4, and measured about two months earlier. The amplitude deviates about 1 dB from the theory and as much as 15 degrees in phase. In this data there appears a definite interference pattern caused by the interaction of two or more signals. The interference could have been caused by an improperly placed piece of absorber in the chamber, or a forgotten metallic object such as a measuring tape in the chamber, but most likely it was caused by the interactions of the incident field with the conductive telemetry lead which may have been improperly led away from the model.

The data as measured with the disc probe are much better and deviate only about 0.5 dB in amplitude and 5 degrees in phase from the theoretical values. In addition to the improved accuracy provided by the disc sensor, there are two other reasons for preferring a disc probe over the monopole. One, the sensitivity of the disc probe is unchanged as the sensor is moved from one location to another as compared to the monopole, whose length and consequently the sensitivity will change; and two, the sensitivity of the disc is usually higher. For example, for the disc as shown in Fig. 6, and monopole of length $h = 0.235$ inch, the sensor signal in the 1-2 GHz frequency range for the disc is about 6 dB above that for the monopole.

As is suggested by the data of Fig. 7, the charge measurement may be susceptible to errors in telemetry lead interactions. So two charge probes that use high resistance telemetry leads were developed and Fig. 9 shows their construction details. Both are built around a miniature microwave detector diode (PD 0911; Parametric Industries, inc.) which has been designed for low capacitance (0.15 pF) and high upper cutoff frequency. At 10 GHz, for example, the diode reactance is about 100 ohms. Physically, the diode has an axial lead package, the glass case being 0.70 inch in diameter (max.) and 0.125 inch long (max.); the leads are 0.014 - 0.016 inch in diameter and about 0.75 inch long. Both probes have 0.5 inch diameter circular bases cut out of a soft copper sheet to permit bending to conform with the surface

Notes:

All dimensions in inches
Diodes: PD0811
Cables: Resistive lead, twisted pair,
   one turn per 2 inches, 40kΩ/ft.

.526

.125

high resistance lead

.50
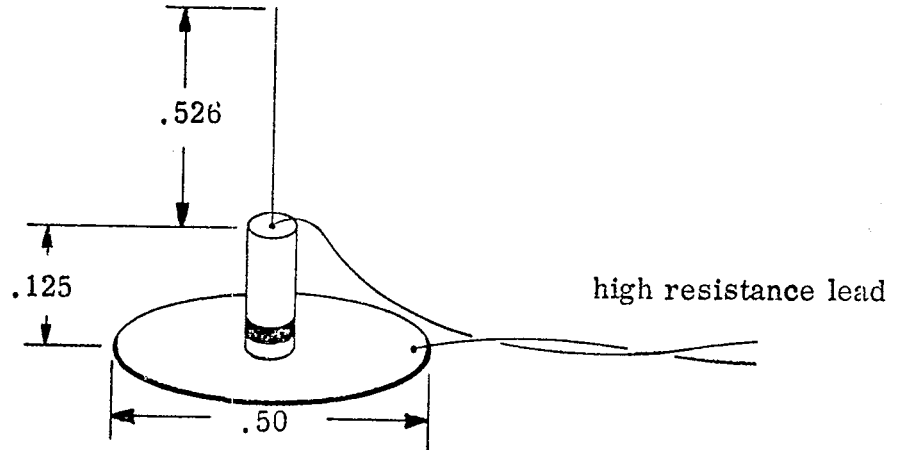
(a) Diode-monopole probe

.156

.140

.50
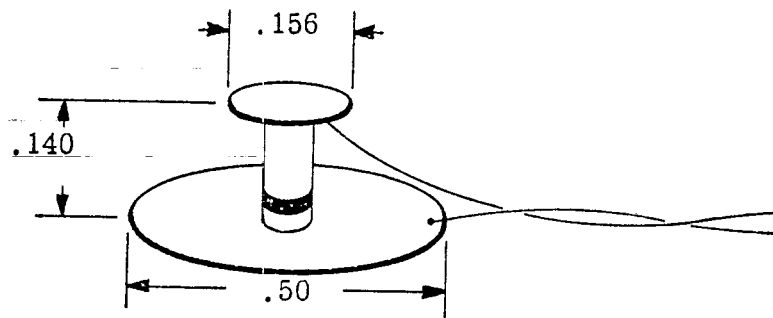
(b) Diode-disc probe

FIG. 9: Self-rectifying charge probes.

of the test object. For the monopole the active portion of the antenna is simply the diode lead cut to about a half-inch length, while for the diode-disc, the sensing element is a 0.156 inch diameter copper disc soldered to the upper diode lead right at the glass envelope. The detected signal is removed from the probe by a 6 ft long twisted pair of high resistance leads[*], one of which is glued with silver paint to the base of the disc and the other to the upper element. When the sensor is mounted on a test object, metallic tape is used to hold the probe to the surface as well as to smooth the surface near the base.

When making measurements with these probes the same facility and most of the equipment is used as with the rf probes. Figure 10 shows the block diagram for the new setup, which differs only in that an rf preamplifier has been replaced by a 1 kHz amplifier-filter combination and instead of the network analyzer or receiver, a Scientific Atlanta (LIN/LOG) Display (Series 1830) is used. In addition, the incident cw signal is now square-wave amplitude modulated at a 1 kHz rate. As the rf frequency is swept the measured signal can be observed on the CRT display or recorded on the X-Y recorder.

The circuit diagram for the amplifier-filter module which we designed and built is shown in Fig. 11. It is used with the diode probes to match impedances and filter the noise outside the narrow band centered at about 1 kHz. It consists of two parts: a broadband low noise amplifier (T_1, T_2) and a 1 kHz active bandpass filter (A_1). In the amplifier section all the gain is provided by the T_1 stage and the T_2 stage is used to provide low impedance drive for the filter circuit which has about $2.7 k\Omega$ input impedance. The $5 k\Omega$ potentiometer in the filter circuit provides frequency tuning from 900 - 1100 Hz, and the 100 kHz potentiometer provides the signal level adjustment to decrease the signal level so as not to overdrive the LIN/LOG module. When the gain setting of the potentiometer is in the maximum position the overall voltage gain of the amplifier-filter unit is 60 dB.

The concept of self-rectifying probes and high resistance leads is not new. In 1962-63 such probes were built at the Radiation Laboratory using then-available

---

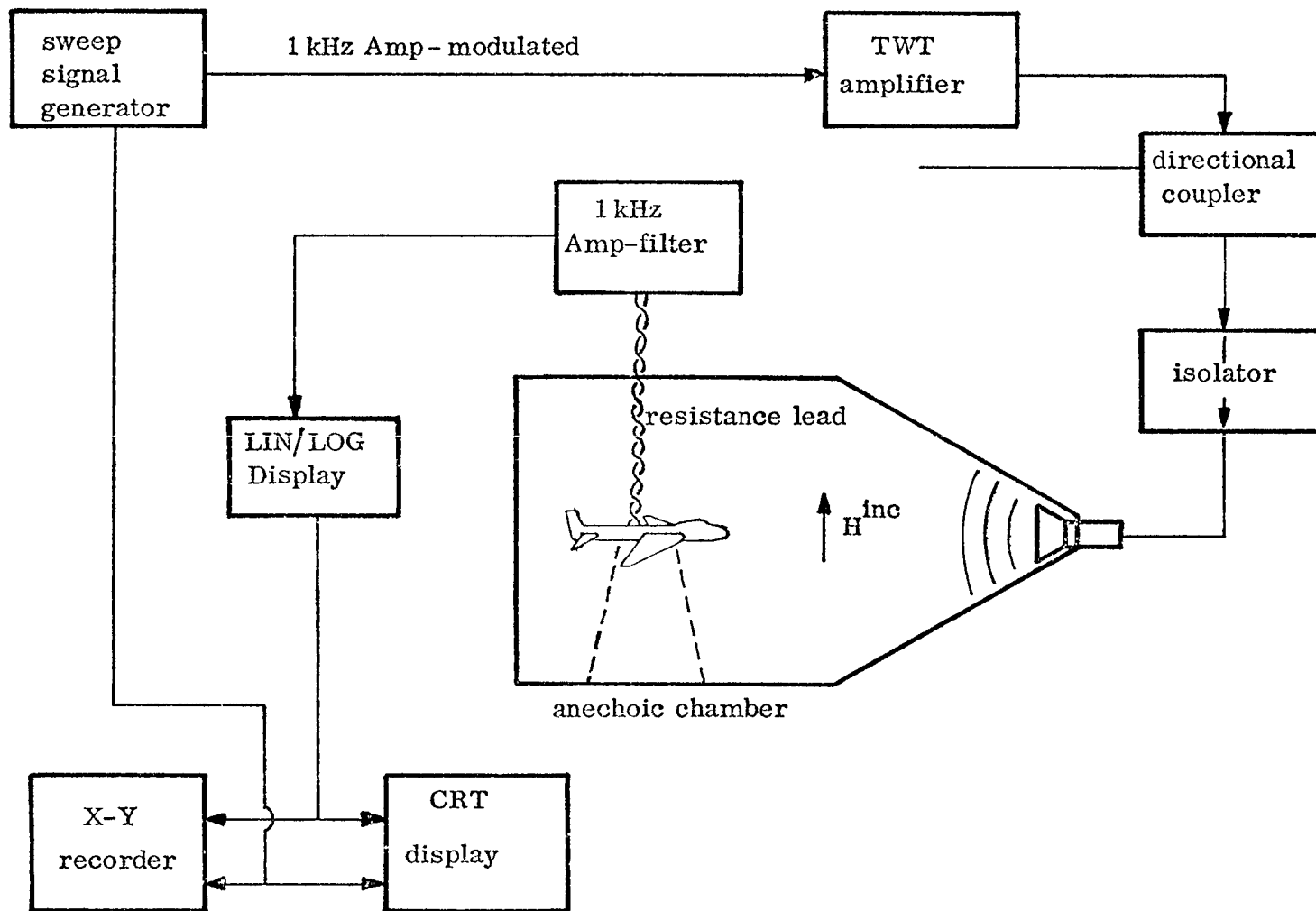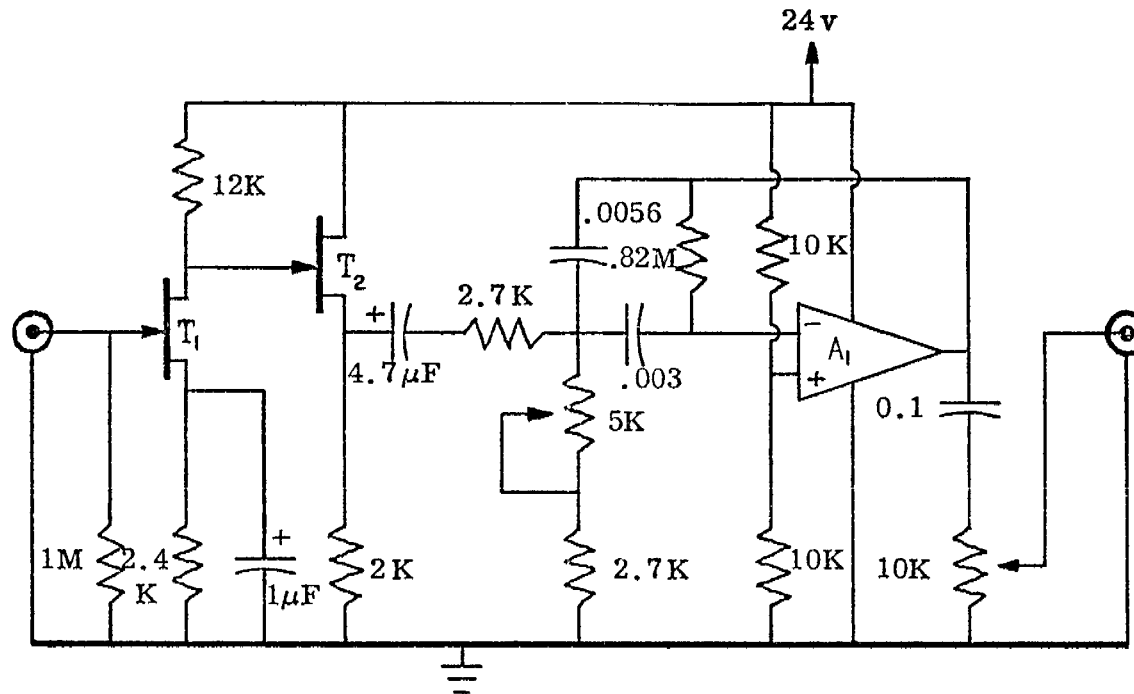[*] Approximately 20 $k\Omega$/ft., single wire. The leads are twisted at about one turn per two inches.

FIG. 10: Block diagram of equipment needed when using diode probes.

T$_1$, T$_2$: Motorola, MPF 105

A$_1$: 741 Op-amp

FIG. 11: Amplifier-Filter for 1kHz signal.

microwave detector diodes (such as 1N21, 1N23, 1N34, etc), but possibly due to their high inherent capacitance (vs. 0.15 pF for the diodes used here) and the larger physical size, the sensitivity was poor and the detection characteristics did not follow a logarithmic curve. Such doubts as to performance were still with us as the new probes were being built, but when the initial results became available, our opinion on the use of diode probes changed.

In Fig. 12 the measured linearity (actually a logarithmic response as detected with the logarithmic detectors) of the diode-disc probe is shown. The measurement was made using the equipment of Fig. 10 and inserting up to three 10 dB attenuators between the isolator and the transmitting antenna. The signal as received by a diode-disc probe was displayed on the Scientific Atlanta (LIN/LOG) Display. The test model in this case was the 6-inch diameter sphere and the frequency was 1.5 GHz. From the curve in Fig. 12 it is seen that for ± 1 dB tracking, the dynamic response of the probe is 27 dB, but if a higher incident power level were available, either by using a higher gain transmit horn or a higher level power (10 w) amplifier, a larger dynamic range could be obtained. Some additional improvement, perhaps a dB or so, could be obtained by a careful manipulation of the amplifier-filter circuit and the twisted pair resistive line; the line appears to be a source of noise pickup, especially the 60 Hz. This would lower the noise level characterized by the horizontal part of the curve. Of course, a larger signal, and consequently a larger dynamic range, would result if larger probes were used, but this would defeat the concept of "electrically small" probes.

The charge as measured with the two diode probes on a 3.133-inch diameter sphere is shown in Fig. 13. The 6-inch sphere was used as the reference and the measurements were made over a 1 - 2 GHz range. We note that in each case, i.e., for the diode-disc and the diode-monopole, the measurement is within 1 dB of the theoretical value; the disc probe shows consistantly lower values, but the results with the monopole are consistantly higher than the theoretical values.

Finally, we remark that the signal received by the diode-monopole was 4 dB above that of the diode-disc in the 1 - 1.5 GHz frequency range and gradually increased

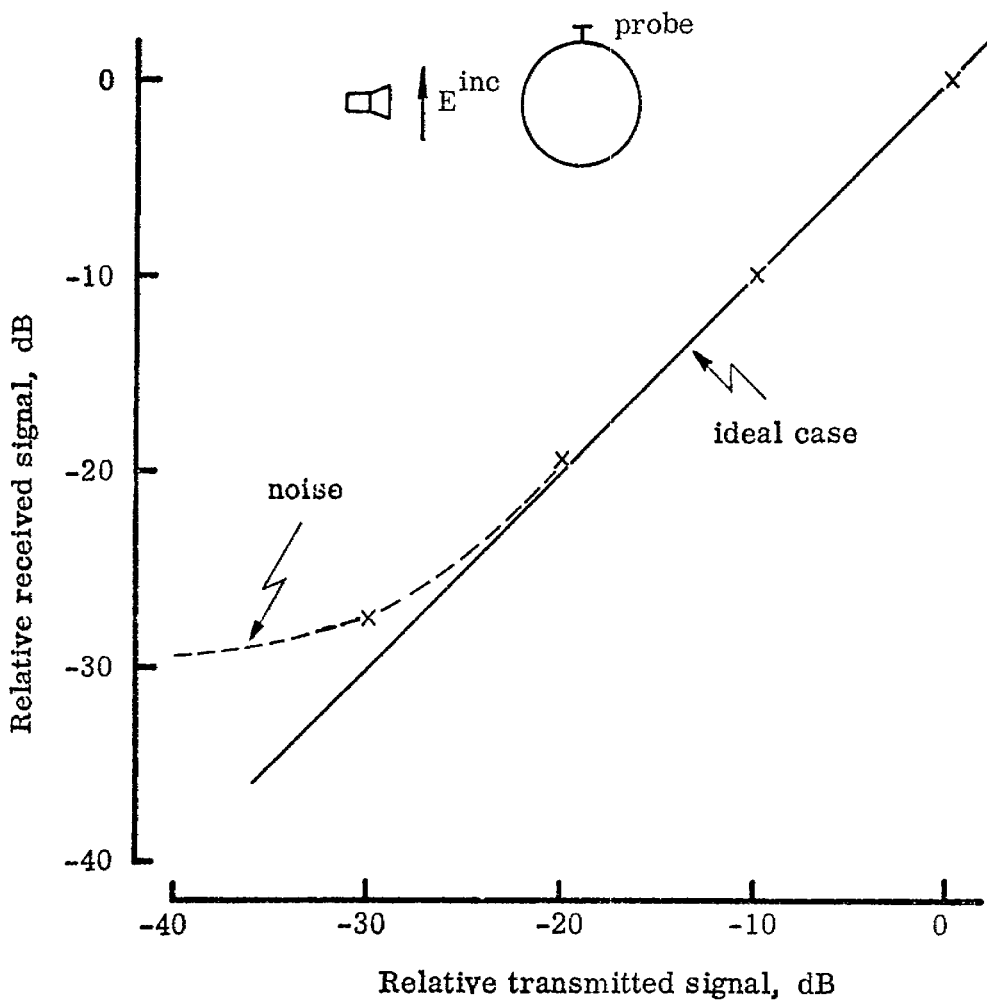FIG. 12: Linearity test of the diode-disc probe measured on
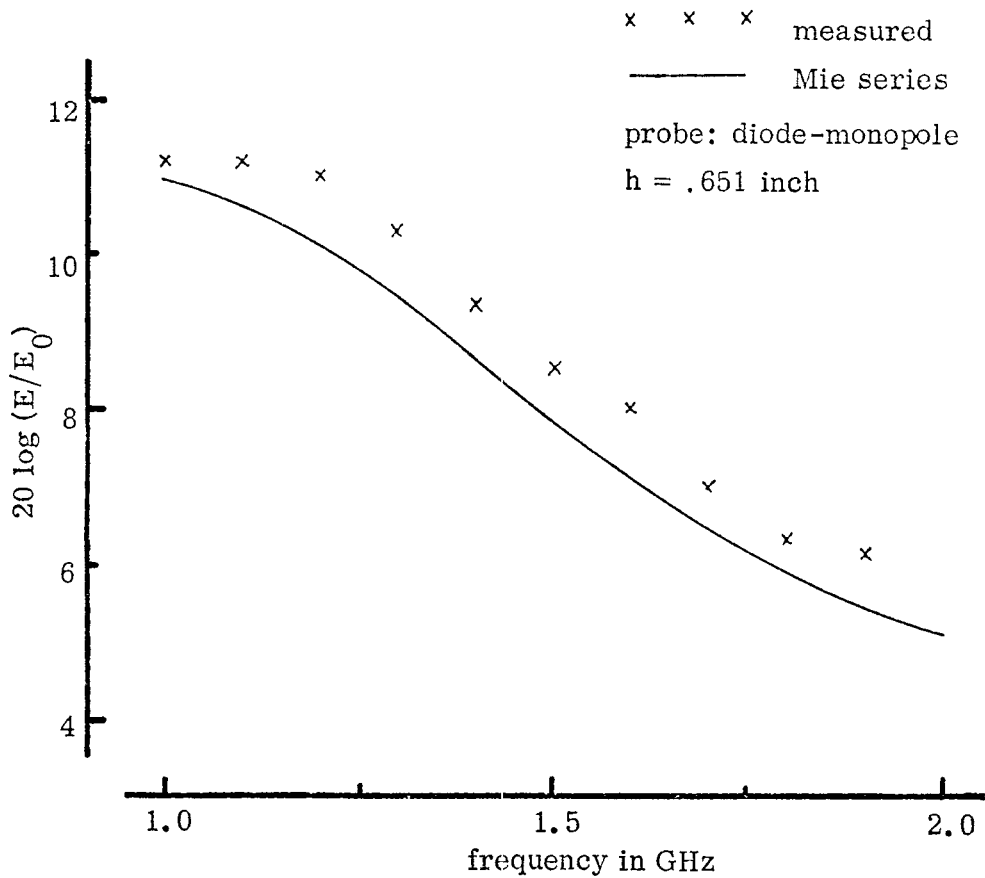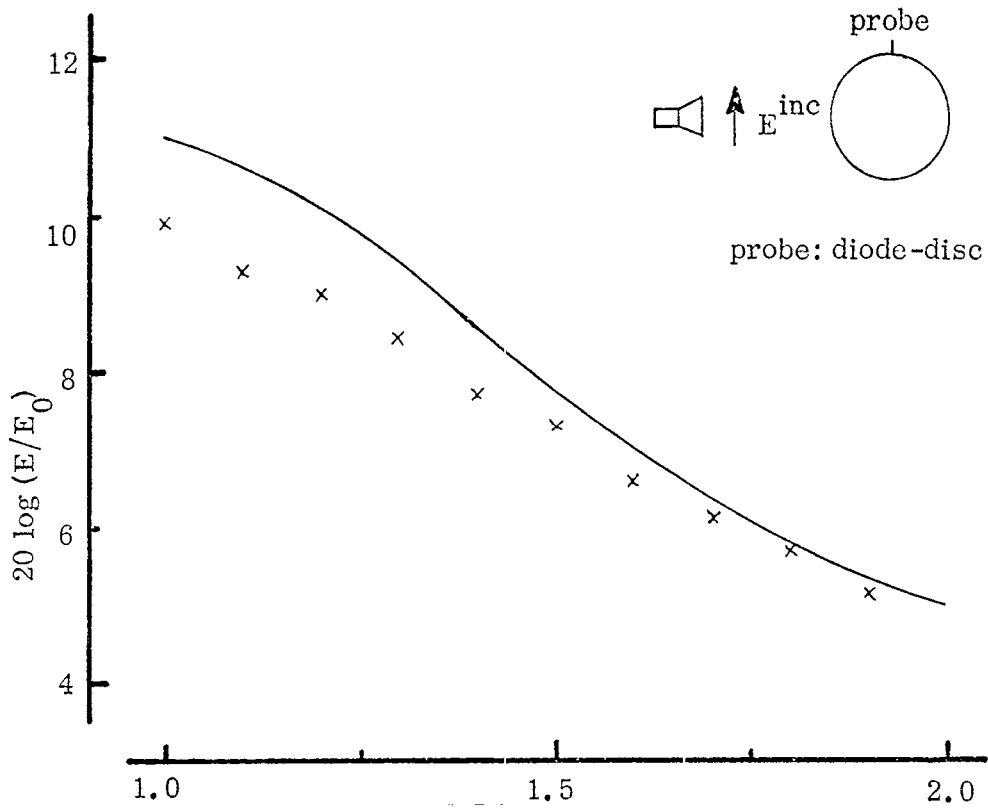a 6-inch diameter sphere.

28

FIG. 13: Charge measurements with resistive lead probes on 3.133-inch diameter sphere.

to 5 dB at 2 GHz. This is opposite to the behavior of the hard lead rf version counterparts. A possible explanation for the lower signal received by the diode-disc is the higher capacitance of the disc structure as compared with the monopole.

SECTION III
EXPERIMENTAL STUDIES

1. INTRODUCTION

In this section the results of experimental studies which were designed to improve and simplify the measurement techniques are presented. The first part reports on the study of the effect of surface perturbations introduced when a lead of a sensor is taped along the surface of the model. The results show that the random variation of data is larger than the perturbations introduced by the lead, and it is therefore concluded that taping the lead along the surface has negligible effect on the measurement accuracy. In the second part the monopole length vs. signal amplitude received is examined. The results agree with theoretical predictions and from these results a method for adjusting data taken by different length monopoles is given. The third topic deals with an experimental study designed to provide correction data for current probes when measurements are made near edges, thin wires, or surfaces of small radii of curvature. Results are available for the case when the currents flow along the edge or the axis of the cylinder. Plans call for an investigation of the transverse case and the development of the related analytical and computer studies as part of a later program.

The last topic deals with the scale model measurements using models made to various degrees of resemblance to the actual model. The results indicate that for low frequency (the first resonance and below) a model of the 747 can be built in about 4 hours out of wood and sheet aluminum on which the induced surface fields will be within the measurement tolerances of the fields on the detailed model.

2. SURFACE PERTURBATIONS DUE TO SENSOR LEADS

When measuring surface charge or current on a body, the measuring device ideally should not introduce perturbations to the electromagnetic field either by the sensor itself or the telemetry of signal lead. However, practical sensing devices are of finite size, are usually made of conductive material, and in most cases will have conductive leads to remove the signal away from the object. In this section a comparison of charge data measured with an internally fed monopole and a taped-on monopole on a 3.133-inch diameter metallic sphere is presented.

Measurements of the normal electric field (i. e., charge) were made on a 3.133-inch diameter sphere using various taped-on and a fed-through monopole. For the latter test, a spherical model was modified to provide the capability of bringing a probe out from within the sphere. The model basically consists of two identical solid aluminum caps joined together by a threaded shaft at the center, but spaced 1/16 inch apart. When a 1/16-inch thick disc of the same diameter as the sphere is inserted and the caps tightened, a solid sphere is obtained. For this spherical model four discs were made, one left intact to make a solid sphere, and in the other three slots were cut to allow the embedding of a coaxial cable. V-shaped slots were cut at 0 and 60°, 0 and 90°, and 0 and 120° in the discs so that when used in conjunction with the sphere and the lead entering at the top, the probe emerged at either 60, 90, or 120 degrees depending upon the disc used.

For each of the three probe positions the charge was measured at 1.2 and 1.8 GHz as the sphere was rotated through 360° in the azimuthal plane. Then the sphere was made solid by replacing the slotted discs with the solid one and the measurements were repeated. But this time the probe and its coaxial lead was taped to the outside of the sphere.

The probe in this case was made by removing a 1/4-inch long section of the outer conductor from the coax end, but leaving the teflon dielectric insulation to provide some mechanical support and protection to the 5 mill diameter center conductor. The coax was then taped to the sphere and the exposed quarter-inch center conductor was bent normal to the surface. To provide a smoother surface at the base of the monopole, a dime-sized disc of metallic tape with a hole in the center was applied over the monopole. The cable was then taped to the sphere with metallic tape and led away from the surface near the top of the sphere. The same measurements were made with the taped-on probe as with the fed-through one described above.

Because of the general similarity of the data for the 60, 90 and 120 degree azimuthal paths and the two frequencies used, results are presented only for the 90 degree or "equatorial" path, and the 1.8 GHz case. In Figs. 14 and 15 amplitude and phase data along with the theoretical values computed from the expression
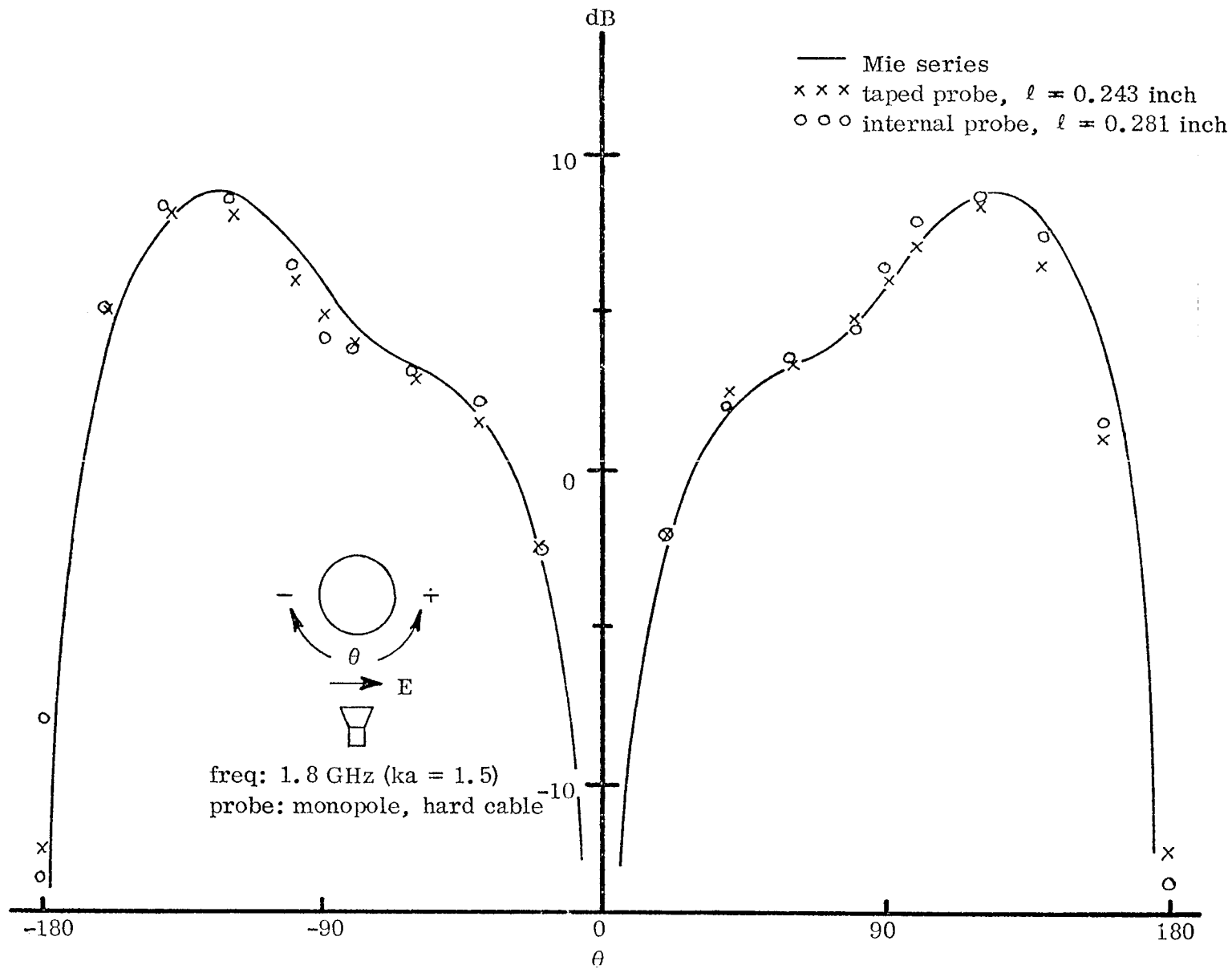
FIG. 14: Charge distribution on a 3.133-inch diameter sphere. The level for the measured values has been adjusted for best fit.

phase, degrees

freq: 1.8 GHz (ka = 1.5)
probe: monopole, hard cable

—— Mie series
× × × taped probe, ℓ = 0.243 inch
o o o internal probe, ℓ = 0.281 inch

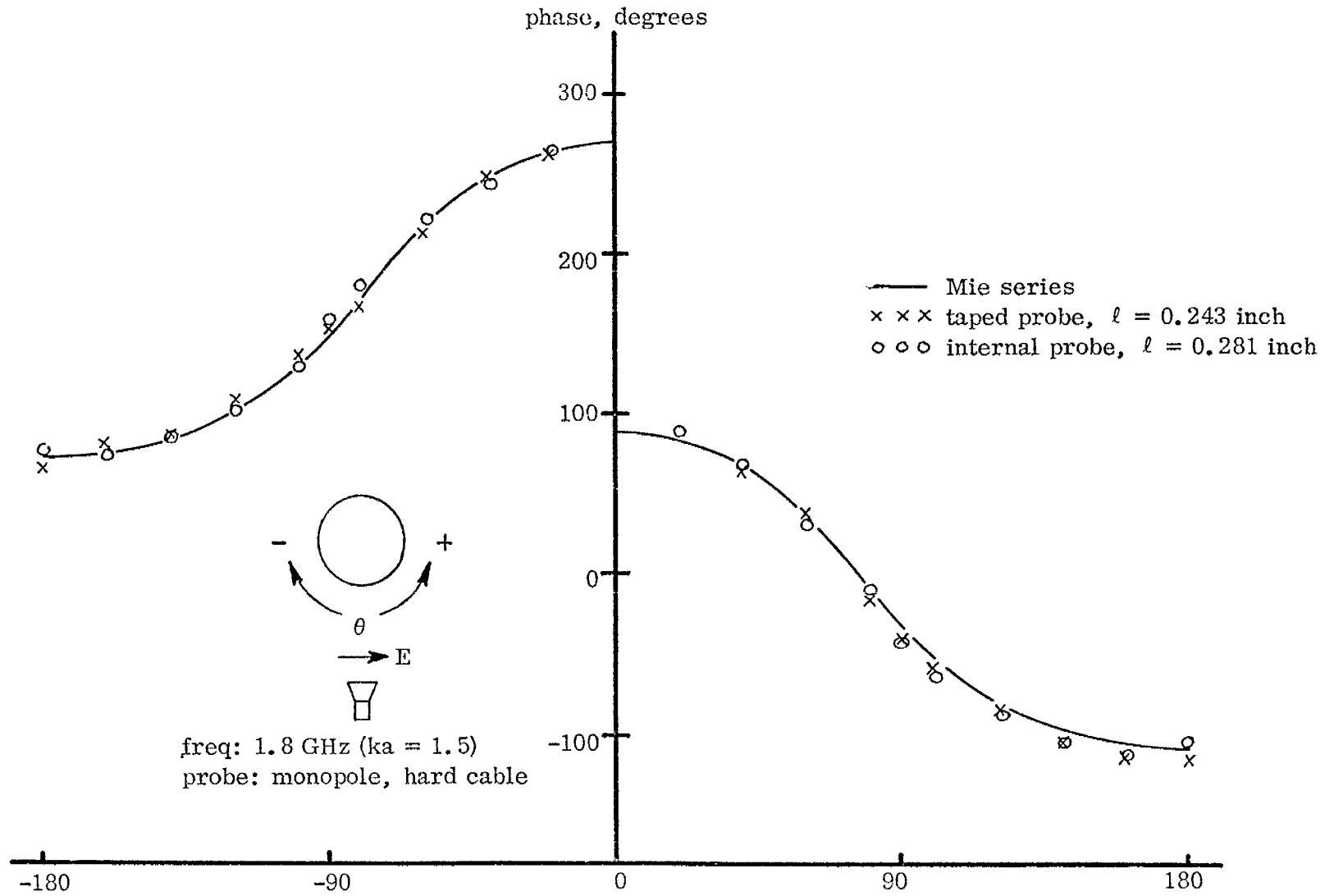FIG. 15: Theoretical and measured phase on a 3.133-inch diameter sphere. The level of the measured
data has been adjusted for best fit.

$$E_r(r=a) = -\frac{\cos\phi}{(ka)^2} \sum_{n=1}^{\infty} i^n (2n+1) \frac{P_n^1(\cos\theta)}{\zeta_n'(ka)} \qquad (1)$$

where a is the radius of the sphere and k is the free space wave number, are presented for 1.8 GHz. In equation (1), $\zeta_n'(x) = \frac{d}{dx}\left[xh_n^{(2)}(x)\right]$ and $P_n^1(\cos\theta)$ is an associated Legendre function as defined by Ref. 4. The time convention $e^{i\omega t}$ has been assumed and suppressed.

Since there is no convenient means of providing calibration for the measured data, the level of the measured curves presented has been arbitrarily normalized, i.e., moved up or down for the best fit with the theory. As is seen, the measured data matches this theory quite well, and where there is a discrepancy, it is believed that it is not caused by the probe response (including taping, etc.), but rather by inaccurate azimuthal rotation of the sphere. It is estimated that the azimuthal positioning accuracy was ±3 degrees.

The spread of data due to inaccuracy of azimuthal positioning of the sphere seems to have caused larger measurement deviation than that introduced by taping the probe to the outer surface of the model. One conclusion, however, can be drawn from this study, and that is that the main source of measurement error in charge measurements will not arise from the taping of the probe but rather from inaccurate alignment of the model in the chamber, and possibly the interaction of the probe lead with the model and the incident field. Therefore, in charge measurements care must be taken to position or tape the probe as accurately as possible on the body and then to align accurately the body with respect to the incident field direction.

3. EFFECT OF MONOPOLE LENGTH ON SIGNAL RECEIVED

A short monopole, made by simply extending the center conductor of the miniature coax, appears to be a good candidate for measuring the normal electric field (i.e., the charge) on perfectly conducting surfaces. Such a sensor is cheap, easy to make, and relatively simple to mount on the surface. (See Fig. 6 for construction details.)

---

4. J.A. Stratton, Electromagnetic Theory, McGraw-Hill Book Co., Inc., New York, 1941, p. 608.

When such a sensor is transferred from one object to another, or even from one place to another on the same model, the tape must be removed and retaped. In so doing, it is very difficult to maintain the same antenna length or even cut the length to a desired value. It is, however, possible to measure the length of the mounted probe to within $\pm$ .002 inch with a depth micrometer, and once the length is known, the measured data can be corrected to correspond to the desired monopole length.

For an electrically short dipole, the antenna impedance is predominately capacitive (ref. 5) , and is given by

$$Z_a \cong 18.3\beta^2 h^2 - j\frac{396}{\beta h} \tag{2}$$

where β is the incident wave number, $2\pi/\lambda$, and h is the total height of the dipole. The corresponding open circuit voltage is

$$V_{oc} = \underline{E} \cdot \underline{h} \tag{3}$$

where $\underline{E}$ is the electric field impinging on the dipole and $\underline{h}$ is the dipole vector height. Translating these values to a monopole geometry of height $h/2$,

$$Z'_a = \frac{1}{2}(18.3\beta^2 h^2 - j\frac{396}{\beta h}) \tag{4}$$

and

$$V'_{oc} = \frac{1}{2}E_n h \tag{5}$$

where it is assumed that the monopole is normal to the surface, and E_n is the normal electric field component.

Since the monopole is feeding a 50-ohm cable (load), the voltage delivered to the load is

5. R.W.P. King, The Theory of Linear Antennas, Harvard University Press, Cambridge (1956), p. 190.

$$V_L = V_{oc} \frac{50}{50 + 9.15\beta^2 h^2 - j\frac{198}{\beta h}}$$

$$= E_n \ell \frac{50}{50 + 1450\ell^2/\lambda^2 - j\,15.85\lambda/\ell}$$

$$\simeq -j E_n 3.15\ell^2/\lambda \quad , \qquad \ell/\lambda \le .03 \tag{6}$$

or simply
$$V_L \sim \ell^2/\lambda \tag{7}$$

where ℓ is the height of the monopole and λ the wavelength of the incident field.

To verify the above relations experimentally, a monopole was fed through the inside of the 3.133-inch sphere model and the received signal was recorded as length ℓ changed from a maximum of 12.8 mm to a minimum of ~ 0 mm. The probe was at the side of the sphere as viewed from the direction of incidence and the measurements were made at 1.0(0.2)2.0 GHz, but at 2 GHz the signal was noisy and unusable.

The resultant data for 1.0, 1.4 and 1.8 GHz are plotted in Fig. 16. Since the incident field was not flat with frequency, no frequency dependence on the signal received can be made. Only the antenna length dependence is examined. From the three frequencies examined, it is seen that the voltage is proportional to ℓ^2 for $\ell^2 \le 0.5$ or $\ell \le 0.7$ cm. Probe lengths commonly used range from 0.22 to 0.250 inch (0.56 to 0.63 cm) and this falls within the region proportional to ℓ^2.

It is straightforward to apply the correction for changes in monopole length. If, for example, for the first measurement

$$\ell_1 = 5.85 \text{ mm} \quad , \qquad s_1 = -45 \text{ dB}$$

but for the second measurement

$$\ell_2 = 5.35 \text{ mm} \quad , \qquad s_2 = -49 \text{ dB}$$

then referenced to $\ell = 5.85$ mm, the second signal

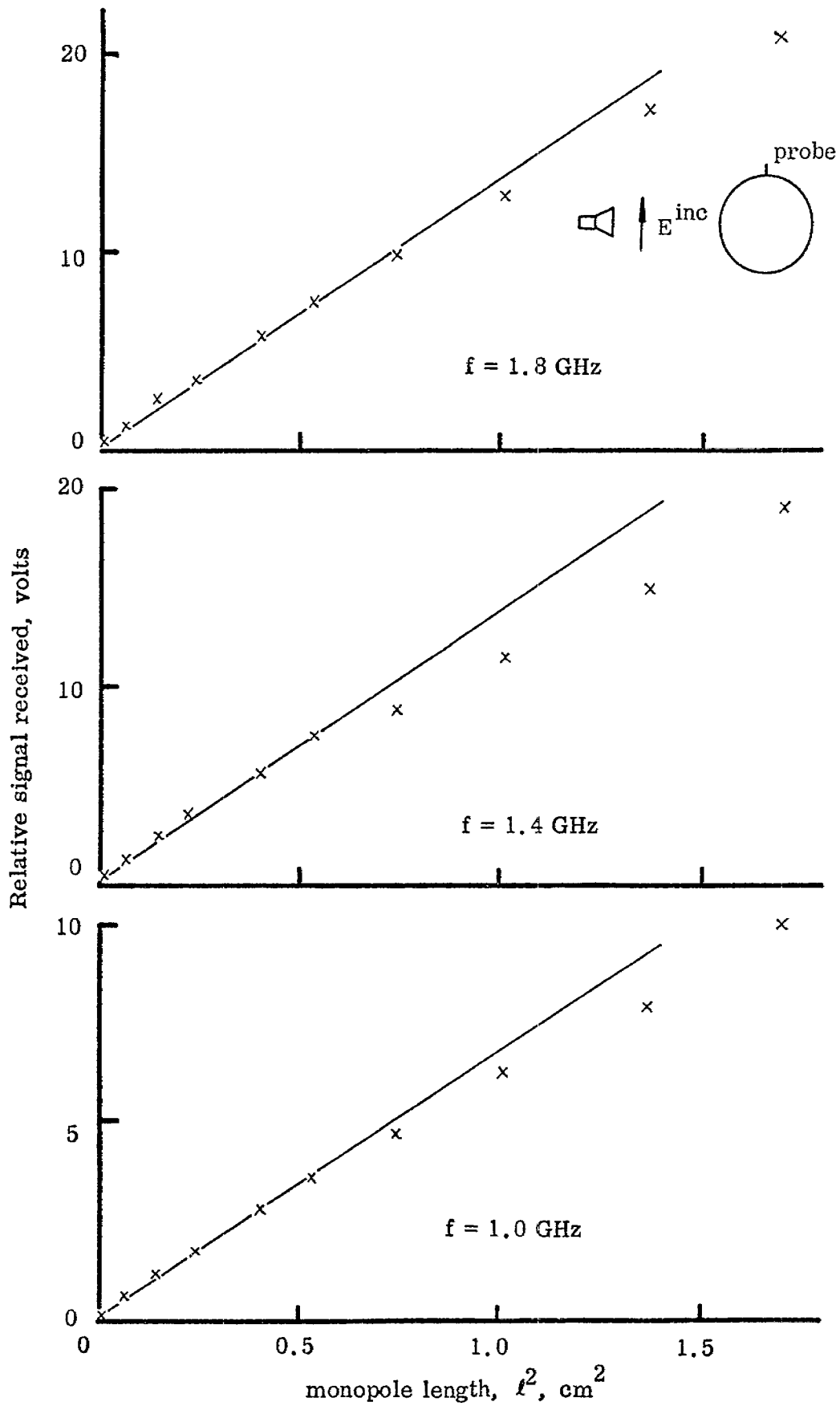$$s_2' = s_2 + 40\log_{10}\ell_1/\ell_2 = -49. + 1.58 = -47.42 \text{ dB}$$

FIG. 16: Received signal vs. monopole length.

4. CALIBRATION FOR LOOP PROBES - EXPERIMENT

The response of a small magnetic loop to an alternating magnetic flux density B is characterized by an integral form of Faraday's Law,

$$\oint_C \bar{E} \cdot d\bar{\ell} = -\frac{\partial}{\partial t} \int_S \bar{B} \cdot d\bar{s} \tag{8}$$

where S describes the surface of the loop and C its boundary edge. When the loop is a single-gap, one-turn device, such as used in our measurements, the voltage V_ℓ delivered from such a loop can be written in the form (ref. 3)

$$V_\ell = -i\omega \frac{Z_\ell}{Z_p + Z_\ell} \int_S \bar{B}_i \cdot d\bar{s} \tag{9}$$

where Z_p is the intrinsic loop impedance, Z_ℓ is the load impedance characterized by a 50-ohm load shunted by the gap capacitance, and $\bar{B}_i$ is the flux density to be measured. For convenience a harmonic time dependence $e^{i\omega t}$ has been adopted and suppressed.

When measurements are made with electrically small loops, it is usually assumed that the magnetic field is constant over the area of the loop and in such case equation (9) becomes

$$V_\ell = -i\omega \bar{B}_i A \frac{Z_\ell}{Z_p + Z_\ell} \tag{10}$$

where A is the effective area of the loop. It is a valid approximation when the radius of the surface curvature of the body on which currents are measured is much greater than that of the loop. It has been found, for example, that for a 0.150-inch outer diameter loop (Probe 211), "errors" larger than 1 dB are encountered when measuring current on cylinders of 0.627-inch diameter.

In view of the fact that magnetic loop probes, however small, will tend to respond to the average value of the magnetic flux over the loop, it is desirable to make

use of that correction or calibration curve for individual probes when measuring skin currents on surfaces of small radius of curvature. To obtain such curves two probes, four cylinders of different diameters, and three frequencies were used. In all cases the incident electric vector was parallel to the axis of the cylinder. This data is intended to satisfy the calibration requirements for the present program and hopefully will provide verification of a theoretical modeling study to predict calibration curves for other probes. The theoretical study has not been completed and therefore is not included herein.

In concept, the procedure for obtaining calibration data for the probes is simple: one measures the current on a body of small radius of curvature for which the theoretical currents are known or can be readily computed and then the difference between the measured and theoretical values is used for the correction for the particular probe, radius of curvature, and frequency used. Spheres, prolate spheroids, finite cylinders (dipoles) and "infinite cylinders" were considered as probable bodies, but after considering various pros and cons of each, an "infinite cylinder" was selected.

To set up an "infinite cylinder" in the chamber, eyelets were screwed into the opposing walls under the absorber and to each eyelet a piece of rope about 12 inches long was tied. A No. 14 wire was tied to the ropes and stretched across the chamber. To provide good tension, a small turnbuckle was used at one end between the rope and the wire. Because the rope is essentially nonconductive, there is no need to remove it when the wire is taken out of the chamber; this saves wear and tear on the absorber panels because they do not have to be removed each time the wire is stretched or removed.

Four pieces of tubing, five feet in length with diameters of 0.193, 0.250, 0.382 and 0.627 in., were used to simulate the infinite cylinder. Each tube, in turn, was threaded over the wire and a metallic tape was smoothly wrapped around the tubing-wire joint to smooth the surface discontinuity. To reduce current reflections from the ends of the wire where it was tied to the rope, a two-foot length near each end was covered with pieces of absorber. Various combinations and arrangements of absorber materials were investigated to

obtain a good match for the currents at the ends of the wire. For the optimum

arrangement the standing wave measured along the cylinder was less than 0.75

dB over a 30-cm span as compared to 2 to 3 dB when other arrangements of

absorber were used. A sketch of the most successful absorber placement is

shown in Fig. 17. The view is from the antenna direction, with absorber
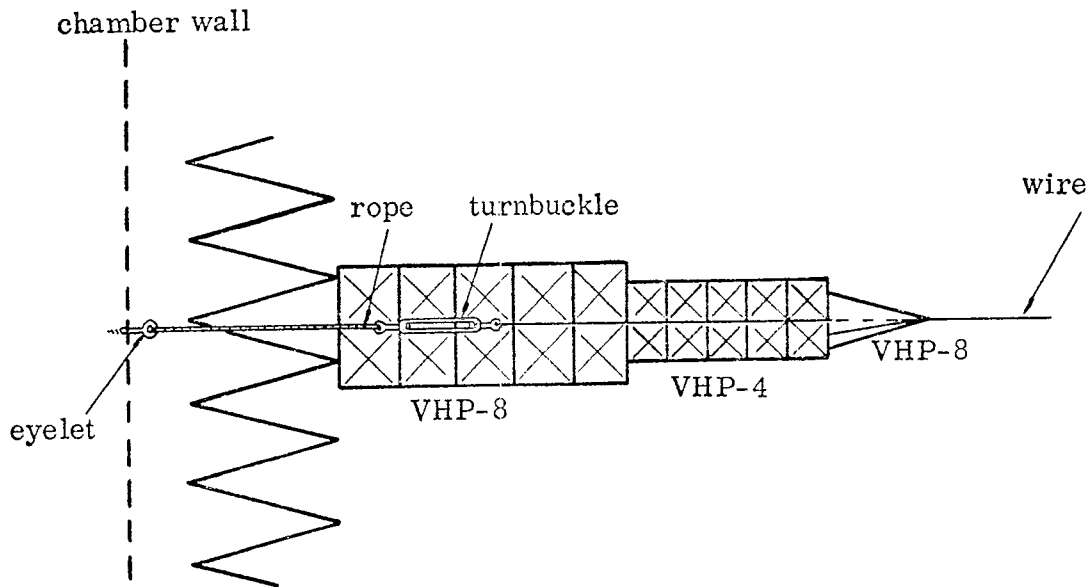
FIG. 17: Absorber arrangement for matching the ends of the wire.
The match is excellent in the 1-2 GHz range.

pyramids pointing toward the transmit antenna direction.

Measurements of current on the four cylinders were made at three

frequencies, 1.0, 1.5, and 1.95 GHz with two probes (see Fig. 18) and the

following measurement sequence was used:

1. Set up a cylinder and a probe in the chamber.

2. Measure current along the cylinder for the three frequencies. This

was done by switching through three preset cw frequencies on the sweep generator

FIG. 18: Dimensions of the probes used.
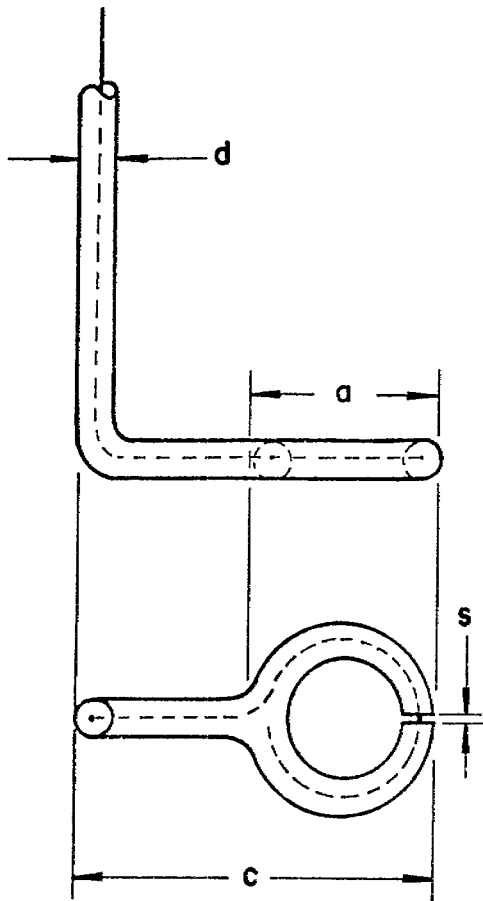
Probe 211

a = 0.122 in.

c = 0.272 in.

d = 0.030 in.

s = 0.1 mm

Probe A

a = 0.304 in.

c = 0.420 in.

d = 0.030 in.

s = 0.1 mm

for each probe position on the cylinder. Data was recorded on two X-Y chart recorders, amplitude on one and phase on the other. The position of the probe along the cylinder was equated to the position on the X-axis on the graph paper. Thus the data points on the graph paper showed the actual current (or phase) standing wave pattern along the cylinder. The current was measured over a span of about 30 cm along the cylinder.

3. Calibrate the incident field. For this, current was measured at the specular points on 3.133 in. and 6 in. diameter spheres carefully positioned in the chamber so that the front of the sphere was in the same plane as the front of the cylinder. Two calibration spheres were used to provide additional accuracy by averaging the incident field values from each sphere. Typically, the difference between the two measurements was 0.1 dB in amplitude and 1° in phase, but discrepancies as large as 1 dB in amplitude and 4° in phase did occur for a few

42

of the measurements.

4. Change the probe and calibrate the incident field (3 above).

5. Measure the current along the cylinder (2 above).

6. Go to 1 and repeat.

To obtain the "infinite cylinder" current value for the cylinder, minimum and maximum values of the current along the cylinder were used. Where the difference was a dB or less, a direct averaging was used, but for larger differences, the dB values were converted to linear scale before averaging. The phase data was recorded on a linear scale thus making averaging straight-forward.

In Figs. 19 through 22 the results of the measurements are presented. No attempt has been made to interpret the data in detail. This has been left for future work when an attempt will be made to correlate these results with theoretically computed responses of the loops in the presence of these cylinders. However, to make the results immediately applicable to aircraft model measurements, theoretical data for infinite cylinders is provided. This was computed from equation (11) on p. 95 of Knott (ref. 1) for which the time convention has been changed from $e^{-i\omega t}$ to $e^{i\omega t}$ and the incident field term $\cos\phi\, e^{ik\rho\cos\phi}$ has been added. As expected, cursory observations of the plots show that the larger diameter probe, Probe A, needs a larger correction, but it also needs a phase correction, which the small probe, Probe 211, does not seem to require.

In application of these results to compensate for the averaging effect of the probe, it has been assumed that the needed correction is independent of frequency. This is indicated by the similarity of the three curves as shown in Fig. 19 for the three different frequencies. Analytical studies (to be reported later) using small argument expansions of Hankel functions also confirms this hypothesis. Thus, for example, if the diameter of the fuselage of the model on which the current is measured with probe 211 is 0.5 inches, the needed correction is the average of the three values or about 1.8 dB, a value applicable throughout the frequency range. No phase correction is needed for this probe, as can be seen from Fig. 19.

relative amplitude in dB

1.95 GHz

theory

phase reference

H^i

loop probe

1.5 GHz

1.0 GHz

cylinder diameter in inches

FIG. 19: Measured (Probe 211) and theoretical current amplitude for cylinder.

44

FIG. 20: Measured (Probe 211) and theoretical current phase for cylinder.
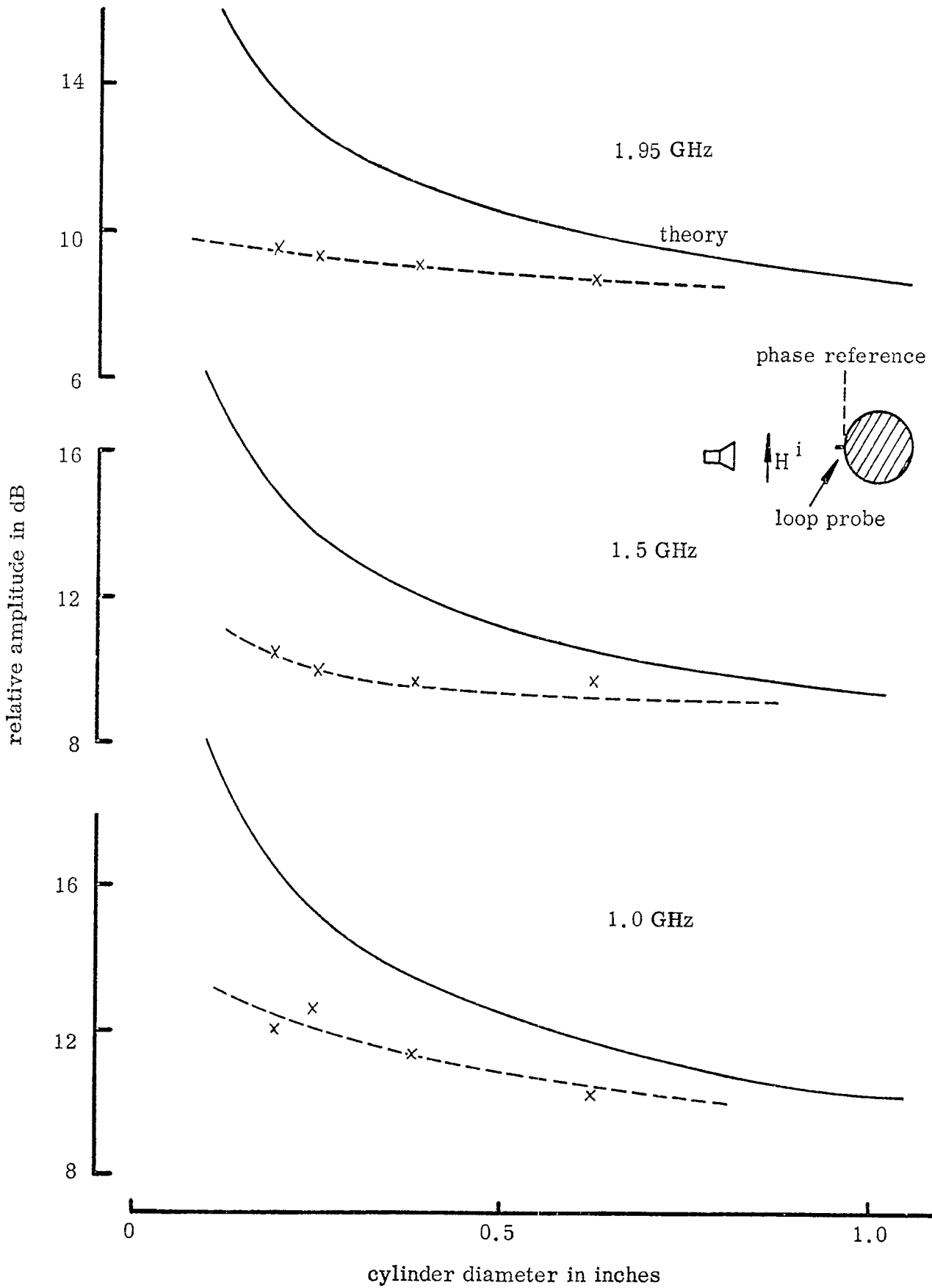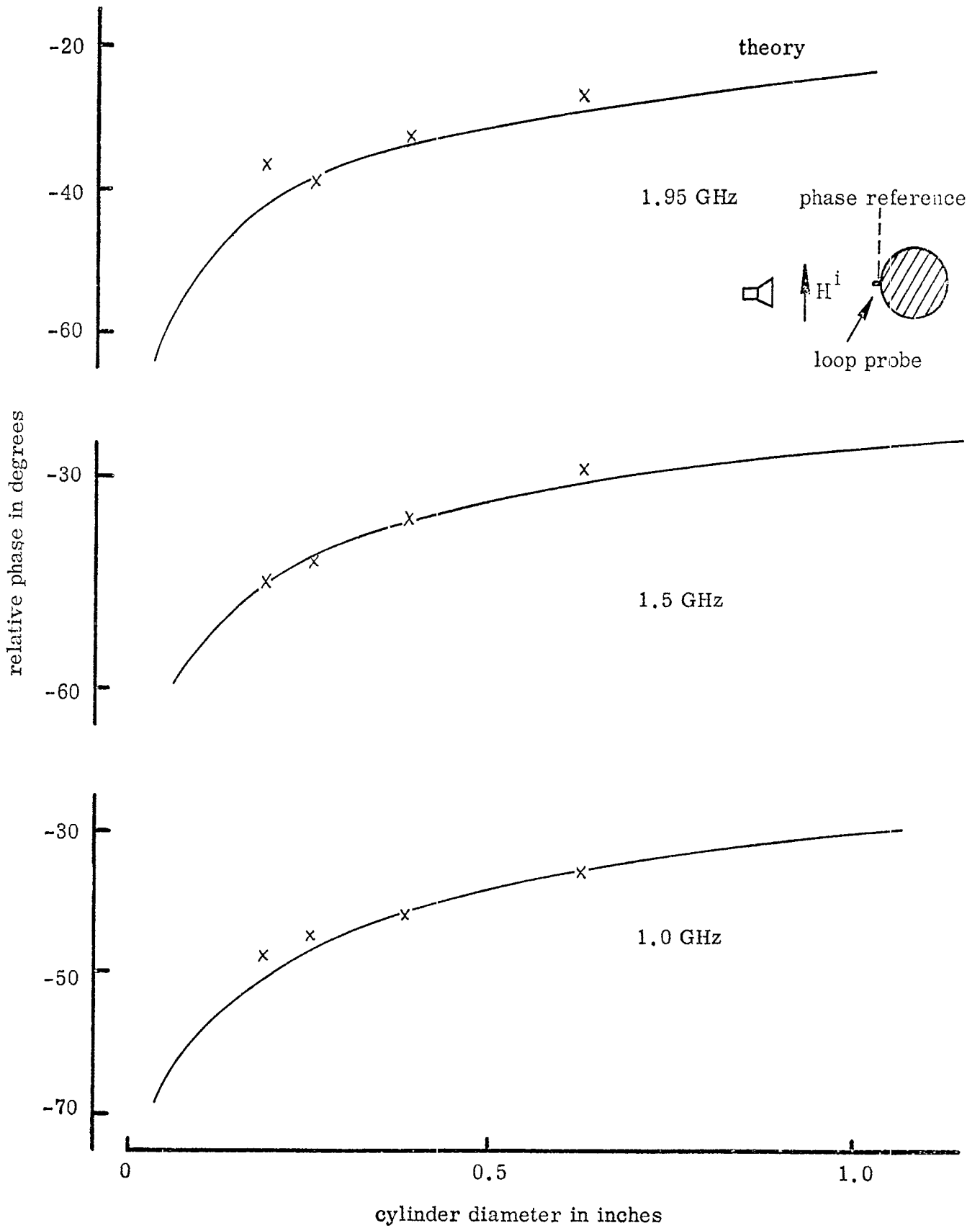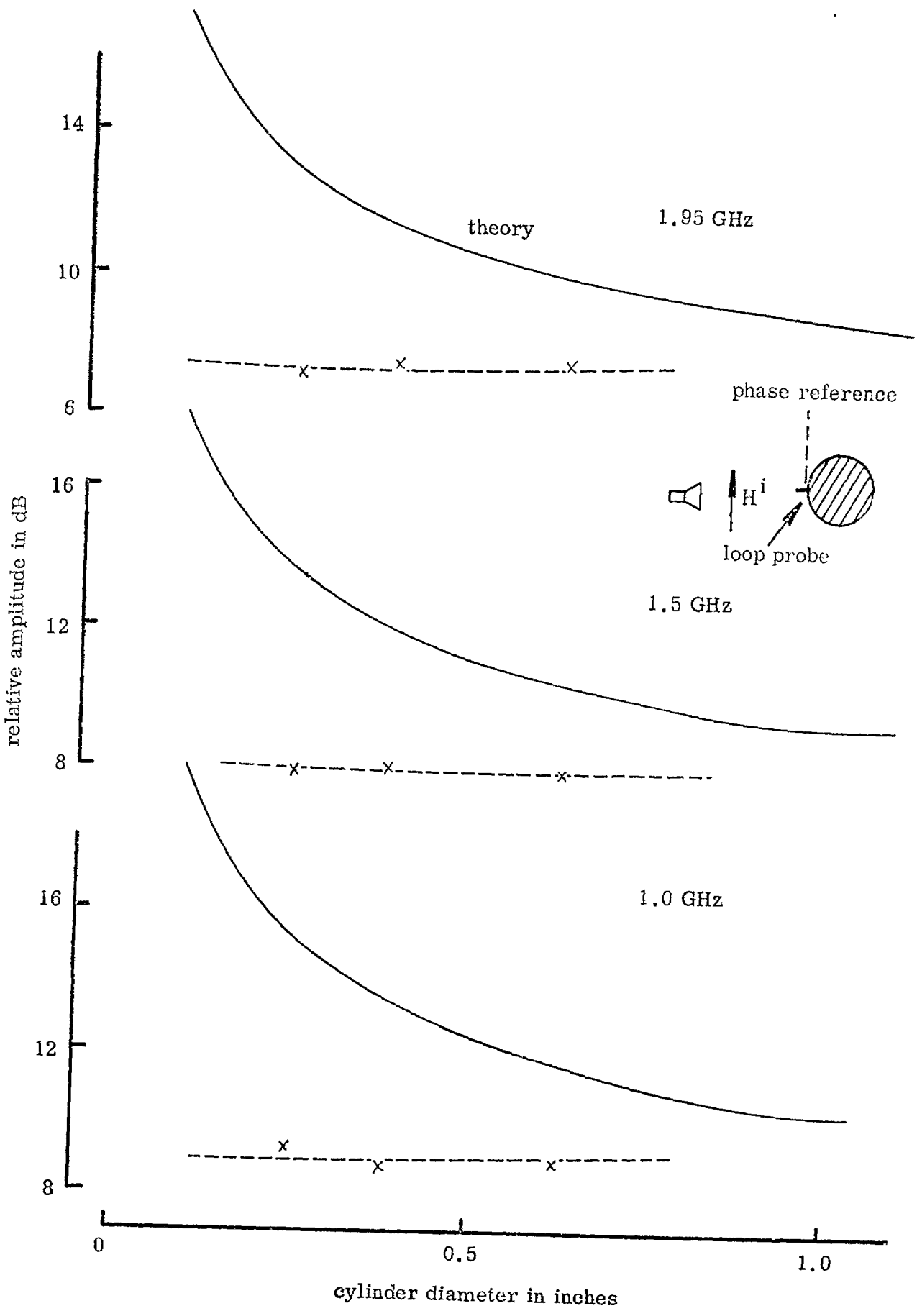
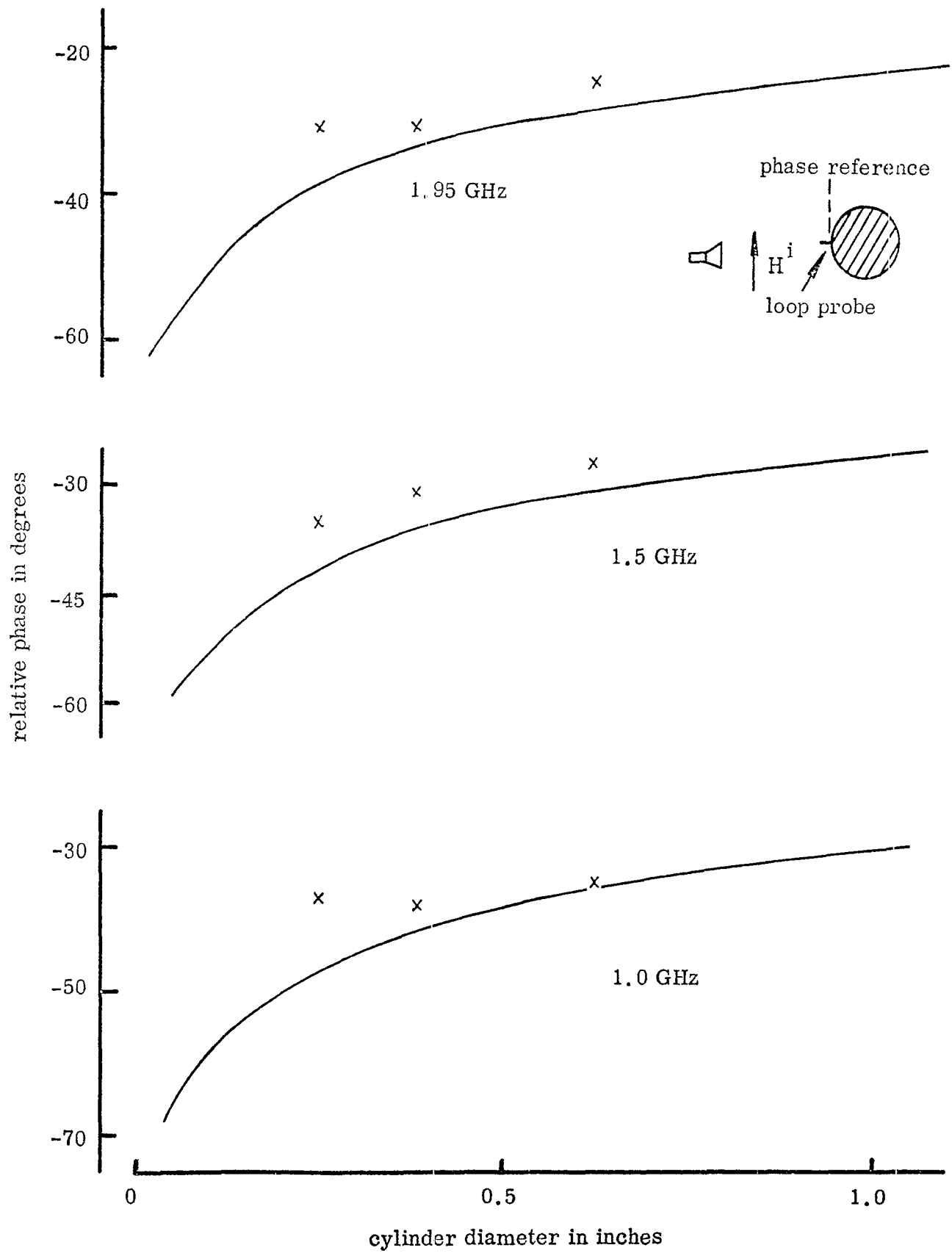FIG. 21: Measured (Probe A) and theoretical current amplitude for cylinder.

FIG. 22: Measured (Probe A) and theoretical current phase for cylinder.

47

5. SCALE MODEL STUDIES

This section is devoted to measurements of skin currents on 747 models built with various degrees of resemblance to the precise shape. The purpose of the study is to provide data to determine to what accuracy the model must be constructed if measurements are to be within a prescribed value of those made on the precise shape model. The emphasis here is on the first resonance and lower, where the precise shape of the model is less critical than at higher frequencies where the skin currents are dominated to a large part, by the local surface geometry.

The skin currents were measured, as a function of frequency, on three 747 models. The models were: (1) a detailed 747 model, (2) rough 747 model (A), and (3) rough 747 model (B). Their shapes and critical dimensions, along with scale factors, are shown in Fig. 23. The scale factors are deduced by comparing the model dimensions with those of EC-747 Advanced Airborne Command Post (AABNCP) whose measurement stations are shown in Appendix A. The detailed model that was used was purchased in a local toy store. It is made of metal (cast aluminum alloy) and on the underside had rubber lading wheels mounted on metal ridges that did not resumble those of the aircraft. Before current measurements were made these wheels were removed and the ridges were filed off to resemble the in-flight configuration.

The rough models A and B were constructed in the laboratory using wood for the fuselage and 1/32 in. thick aluminum sheet metal for the wings and vertical stabilizers. The models were painted with conductive silver paint. The model A was designed to be of a close resemblance to the detailed model. Its fuselage is a circular cylinder of diameter equivalent to that of a 747 at the midpoint of the fuselage. The wings and tailfin are also shaped to those of the actual model, but do not have the engines nor the broken trailing edge for the front wings. The fuselage ends were rounded to resemble those of the aircraft, but the wing and tailfin edges were left squared.

The model B is a rougher model of the 747 aircraft. Its fuselage was

(a) Detailed 747 model

9.40

1.44

2.86

7.83

Scale: 1/730.1 (length)
1/761.7 (width)

(b) Rough 747 model A

10.18

0.63

2.41

1.59

0.97

3.20

8.82

0.41

0.69

Scale: 1/674.2 (length)
1/676.2 (width)

(c) Rough 747 model B

9.42

0.96

1.34

1.35

3.58

7.97
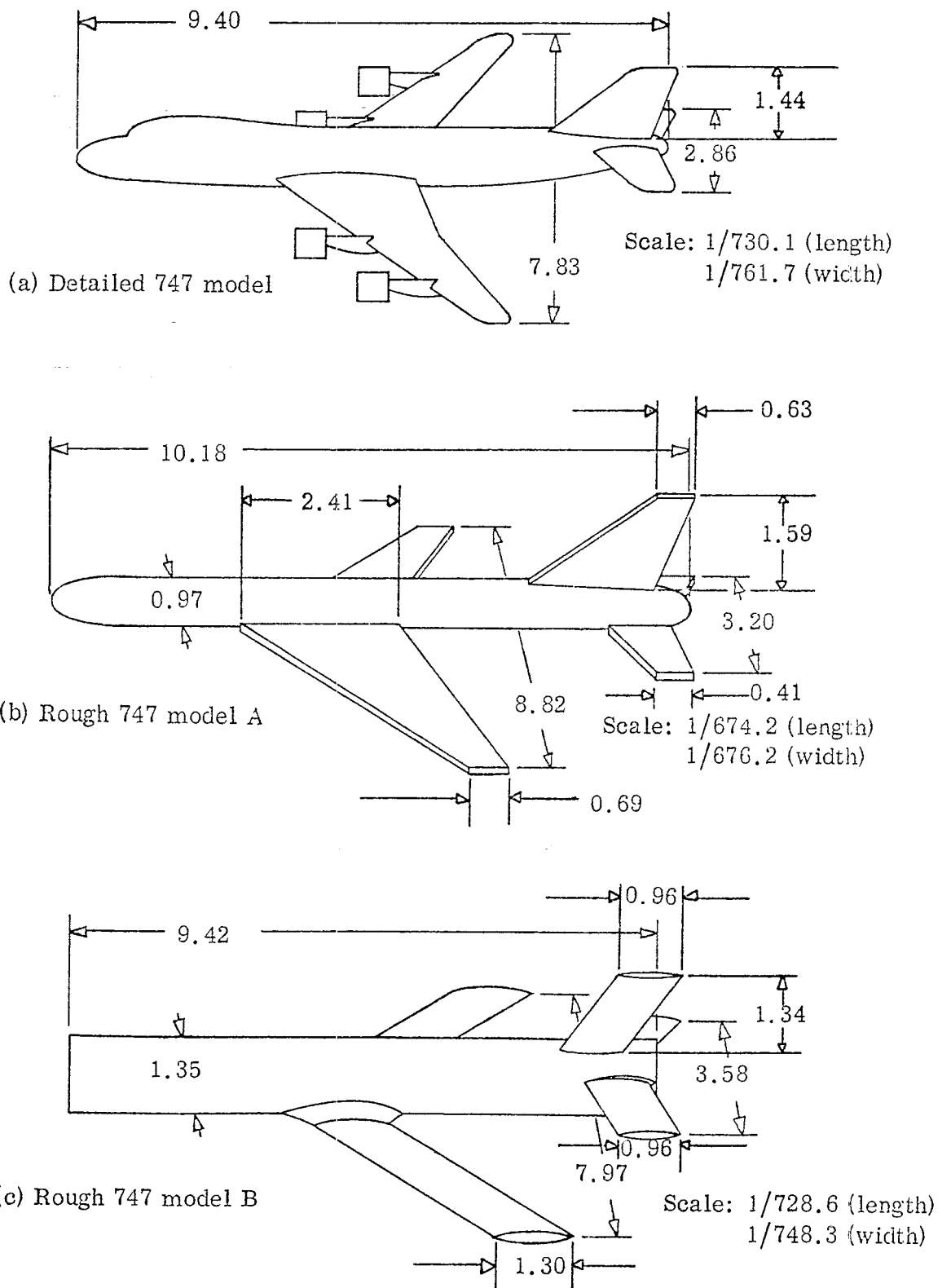
0.96

1.30

Scale: 1/728.6 (length)
1/748.3 (width)

FIG. 23: Scale models of various resemblance; dimensions in
centimeters.

made of a larger diameter wood dowel whose ends were intentionally left flat. The wings were made of 1/32 in. thick aluminum sheet, but filed to an elliptic shape. Also note that the wings and stabilizer are not tapered as in the detailed model and model A.

For the three models the skin currents were measured at the midpoint of the fuselage, STA = 1440 (see Appendix A), top and bottom, and in each case the current was measured on the illuminated side of the model. When the incident electric vector was parallel to the fuselage, the currents along the fuselage were measured, but when the polarization was changed, i.e., the incident electric vector was normal to the fuselage, the current flowing across the fuselage was measured. The direction of incidence and polarization and the current components which were measured are shown by the insert sketch on each of the figures where data are presented.

The measurements were made by sweeping 1-2 and 2-4 GHz ranges to cover the 1-6 MHz range, and 1-2 GHz range to cover the 1-3 MHz range. Probe 211 was used in these measurements and the probe correction data (Section III.3) was applied to the case of top fuselage currents excited with the incident electric field parallel to the fuselage (Figs. 23 and 24). The similar currents measured on the bottom of the fuselage were not corrected because due to the presence of wing roots the effective surface curvature there is almost flat. In the case of perpendicular polarization, amplitude correction was not made since for such the correction data are not yet available. However, due to the flatness of the surface on the bottom of the models it is expected that little or no correction would be needed there, but for the top of the fuselage where a cylindrical shape is definitely dominant, a one or two dB adjustment may be needed.

Figures 24 and 25 show the current amplitude and phase on top of the fuselage, illuminated from the top with the electric vector parallel to the fuselage. As seen from the amplitude curves, the detailed model and the model A resonate at 1.75 MHz, but model B resonates at about 1.63 MHz. The reason for the lower resonance of model B is its fat fuselage. The behavior here is similar to that of a half-wave resonant dipole — the fatter
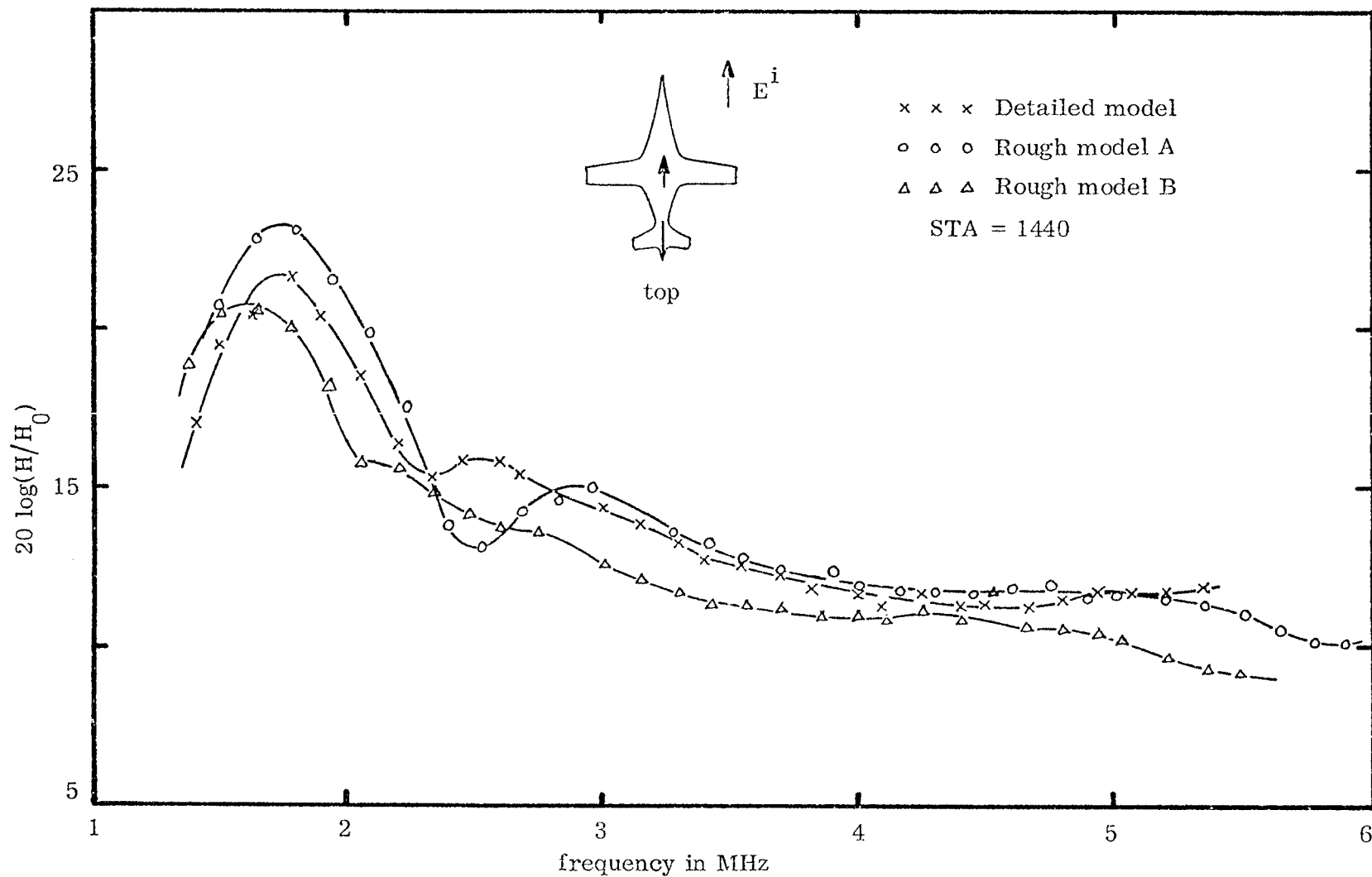
FIG. 24: Current amplitude at the midpoint of the top of the fuselage of the 747 models; top illuminated, E^i parallel to the fuselage
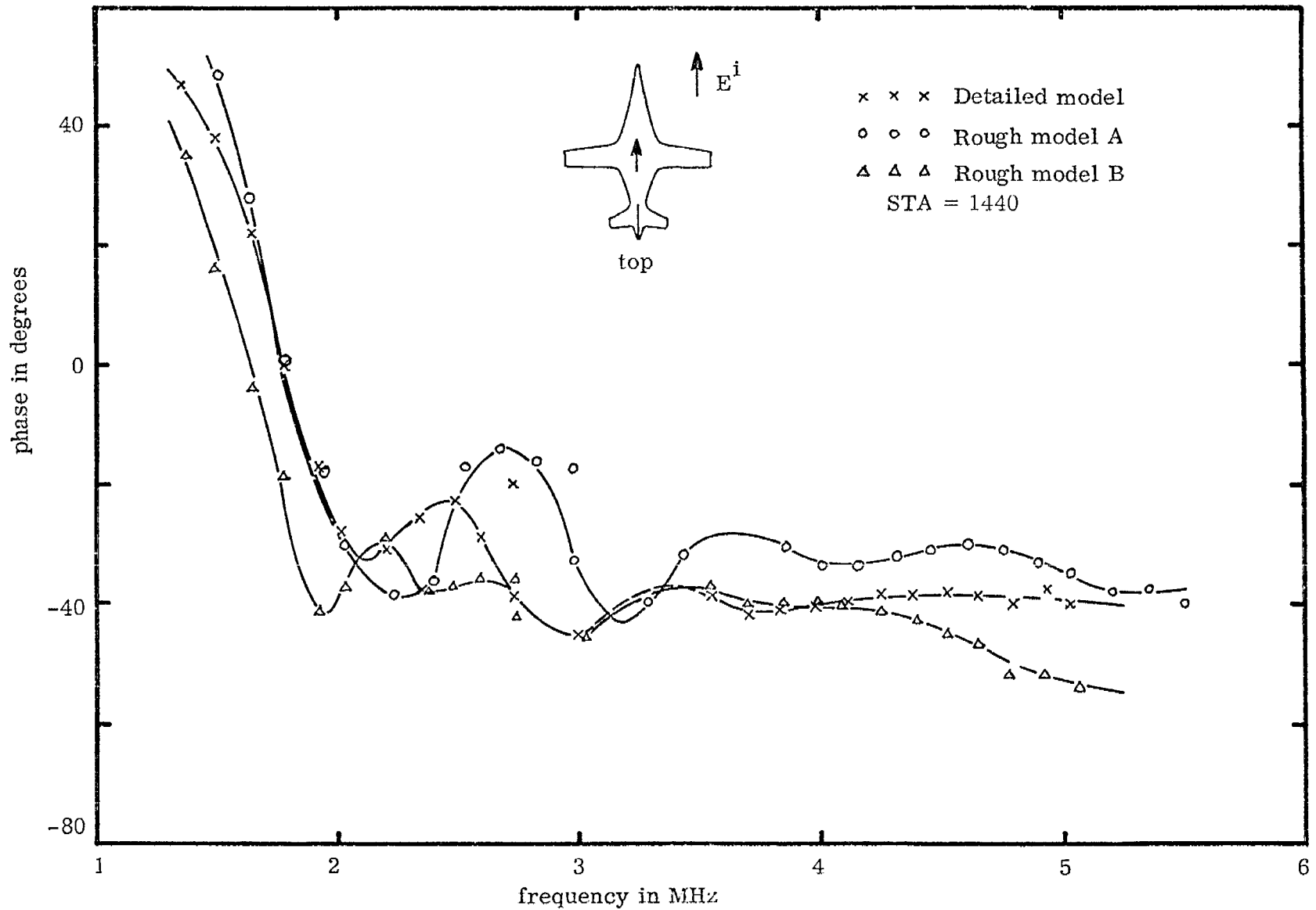
FIG. 25: Current phase at the midpoint of the top of the fuselage of the 747 models; top illuminated, E^i parallel to the fuselage. Phase reference is top of fuselage.

the dipole the lower the resonant frequency, and also the lower the surface current density. The 1.5 dB higher current amplitude measured on model A than on the detailed model can be explained by the fact that model A has a smoother shape, implying a higher Q structure.

Figure 26 shows the current measured on the bottom of the fuselage, with incident electric vector parallel to the fuselage. A comparison of this data with that for the top of the fuselage shows a great similarity for both the amplitude and phase, the only difference being the 7 dB (about) lower amplitudes for the bottom measurement. The difference is real, and results from the fact that the flat bottom surface has a tendency to spread the currents and thus decrease the current density.

Figures 27 and 28 show the measured current on the top and bottom of the fuselage, respectively, with the incident electric vector normal to the fuselage. Note that now the currents on top of the fuselage are about 5 dB lower than those for the bottom, which is opposite to that observed for the other (parallel) polarization. This behavior can be explained by the fact that for the perpendicular polarization the dominant currents are supported by the wings and the bottom surface being flat offers less opposition to the current flow than does the top of the model which has a cylindrical hump (fuselage). It should also be remembered that since the probe calibration data for perpendicular polarization is not available, no correction has been made. It is expected that such correction will raise the level of current measured on top of the fuselage.

No attempt is made here to assess the results or to determine a criterion for construction of rough scale models to be used for surface field measurements when commercial or detailed models of required scale are not available. To deduce such criteria one must first know the accuracy (in amplitude, phase and frequency) which the rough model must provide, and one must also know which measurements will be made on the particular model. For example, if the fuselage resonance is to be studied, a model such as model A would suffice, but such a model would be inappropriate when wing resonances
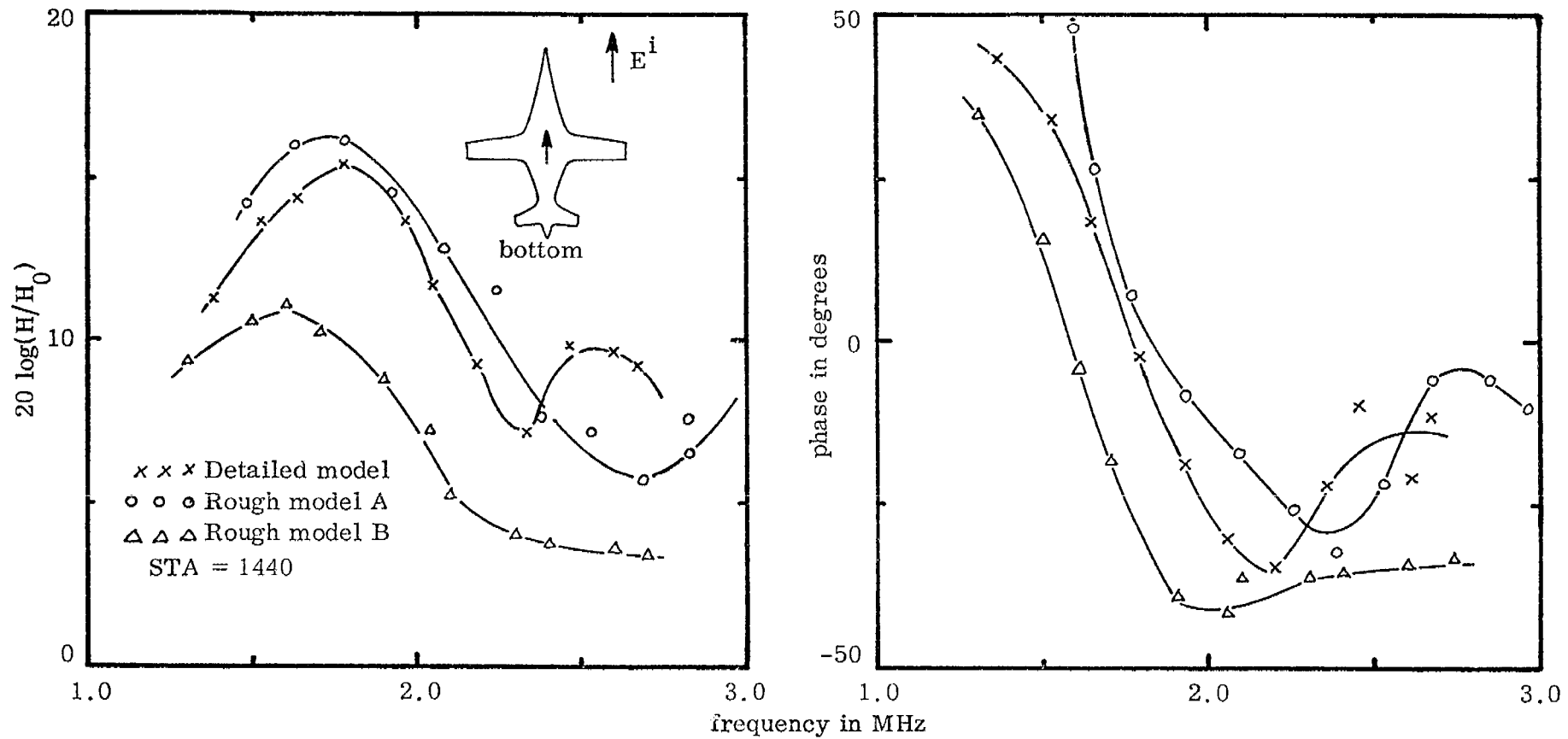
FIG. 26: Current amplitude and phase at the midpoint of the bottom of the fuselage of the 747 models; bottom illuminated, E^i parallel to the fuselage. Phase reference is bottom of fuselage.
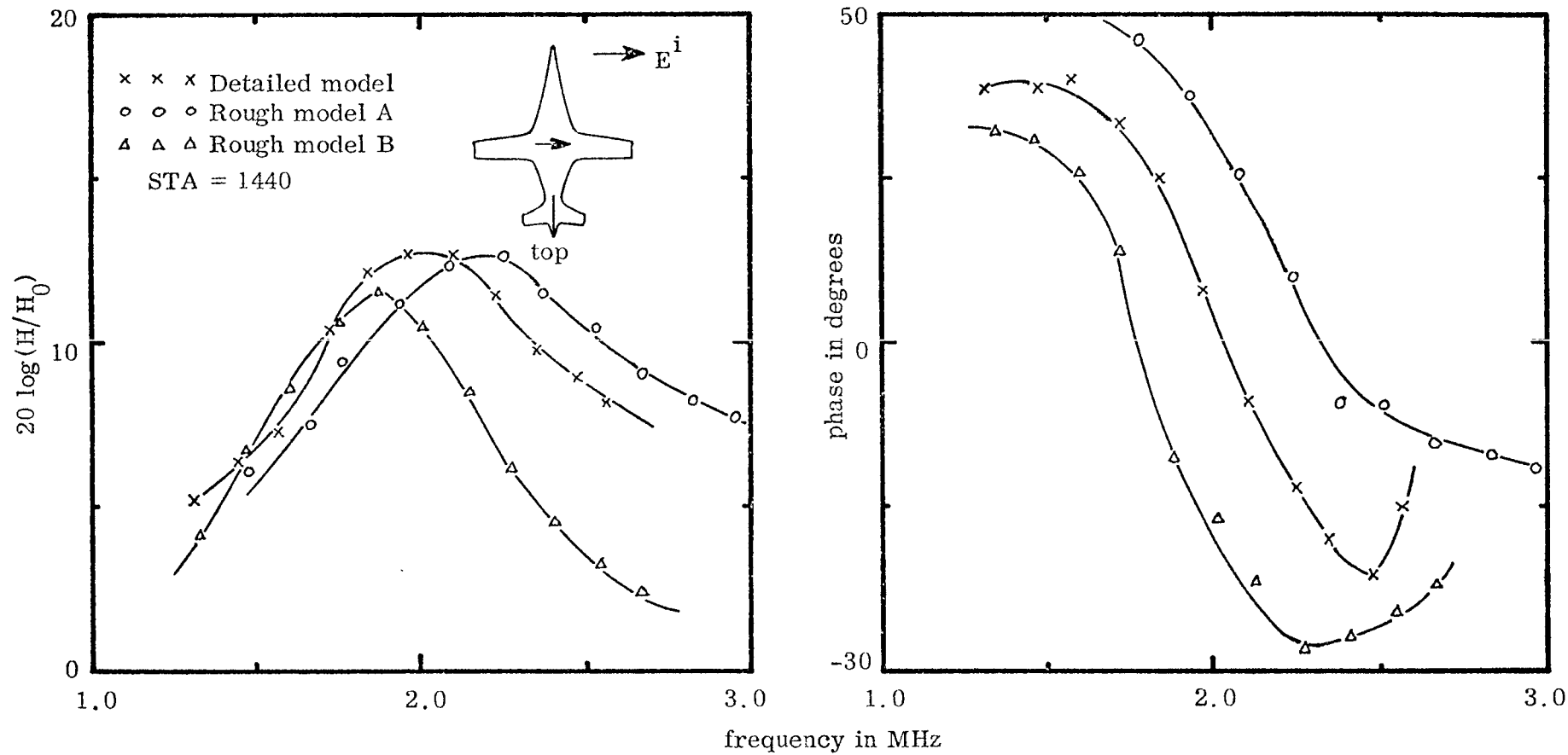
FIG. 27: Current amplitude and phase at the midpoint of the top of the fuselage of the 747 models; top illuminated, E^i perpendicular to the fuselage. Phase reference is top of fuselage.
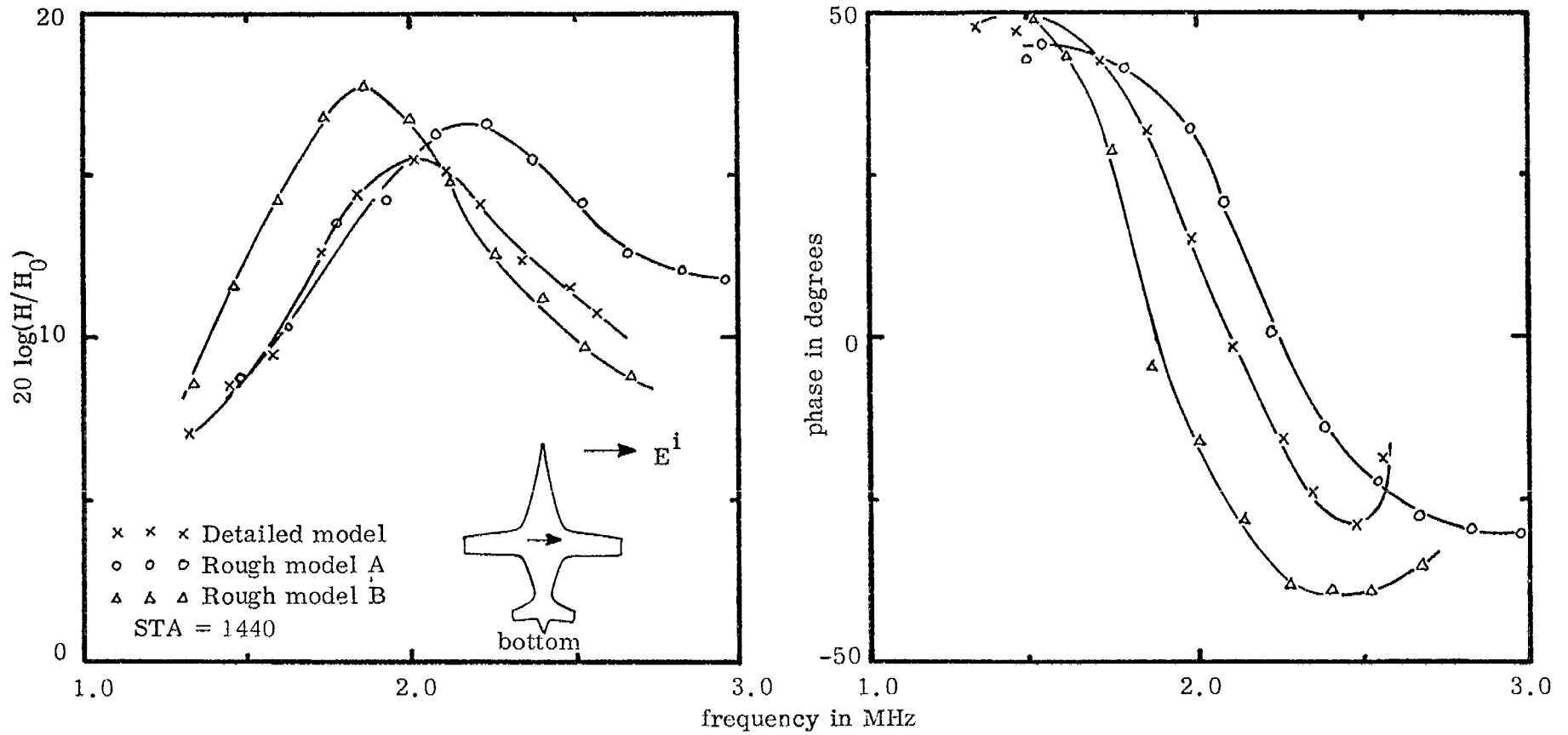
FIG. 28: Current amplitude and phase at the midpoint of the bottom of the fuselage of the 747 models; bottom illuminated, E^i perpendicular to the fuselage. Phase reference is bottom of fuselage.

are to be determined. Recall that the data for the detailed model showed lower resonance than Model A (see Fig. 27), indicating that for such a case the presence of engines does affect the resonance behavior.

SECTION IV

WIRE GRID MODEL MEASUREMENTS

In this section, the investigation of the amplitude and phase of the skin currents on wire grid models is discussed and the experimental results are presented. The models used are the so-called wire grid models used by Taylor (ref. 2) for computation of currents for a B-1 aircraft. The dimensions for the two models used are shown in Fig. 29, with wings forward and wings swept. The laboratory models were made of brass by machining cylinders of required diameters, lengths, and end shapes, after which the pieces were joined with solder to form the model. The 1/239.3 scale factor for the model resulted from selection of 5/8 in. diameter standard brass stock for the fuselage.

For the two models, wings forward and wings swept, surface current amplitude and phase was measured for five different cases and these are listed in Table 1 along with the corresponding figure numbers (30-39) which show data curves. In each figure the data is presented for two cases, wings forward and wings swept, with all other conditions being the same. The station (STA) numbers designate location of the particular measurement and those for the fuselage are measured (in meters) from the nose of the aircraft and for the wings the measurement is made from the root of the wing, specifically, from the point where the axis of the (cylindrical) wing intersects the axis of the fuselage. The (F) or (W) after the station number refers to the fuselage or wing station, respectively.

The measurements were made using the No. 211 loop probe and for calibration two measurements were made, one with the 3.133 in. diameter and the other with the 6-in. diameter sphere. The incident field value was obtained by averaging the values obtained from two measurements which, on the average, deviated only 0.25 dB for the amplitude and 2.3° for the phase. An amplitude correction factor of 1.17 dB, appropriate to 0.625 fuselage diameter, has been added to data in Figs. 30, 32, and 34, and a 2.27 dB correction factor, appro-

58

(Drawing not to scale.)

STA(W), m.

STA (F), meters

21.6 m (3.554)

24.5m (4.031)

1.1 m (.362)

0.72 m (.237)

8.5 m (1.398)

80.5° 40.5° 59°

19.6m (3.225)

12.8m (2.106)

8 m (1.316)

24.5m (4.031)

35°

8.5 m (1.398)

1.4 m (.461)

2.63 m (.433)

3.8 m (.625)
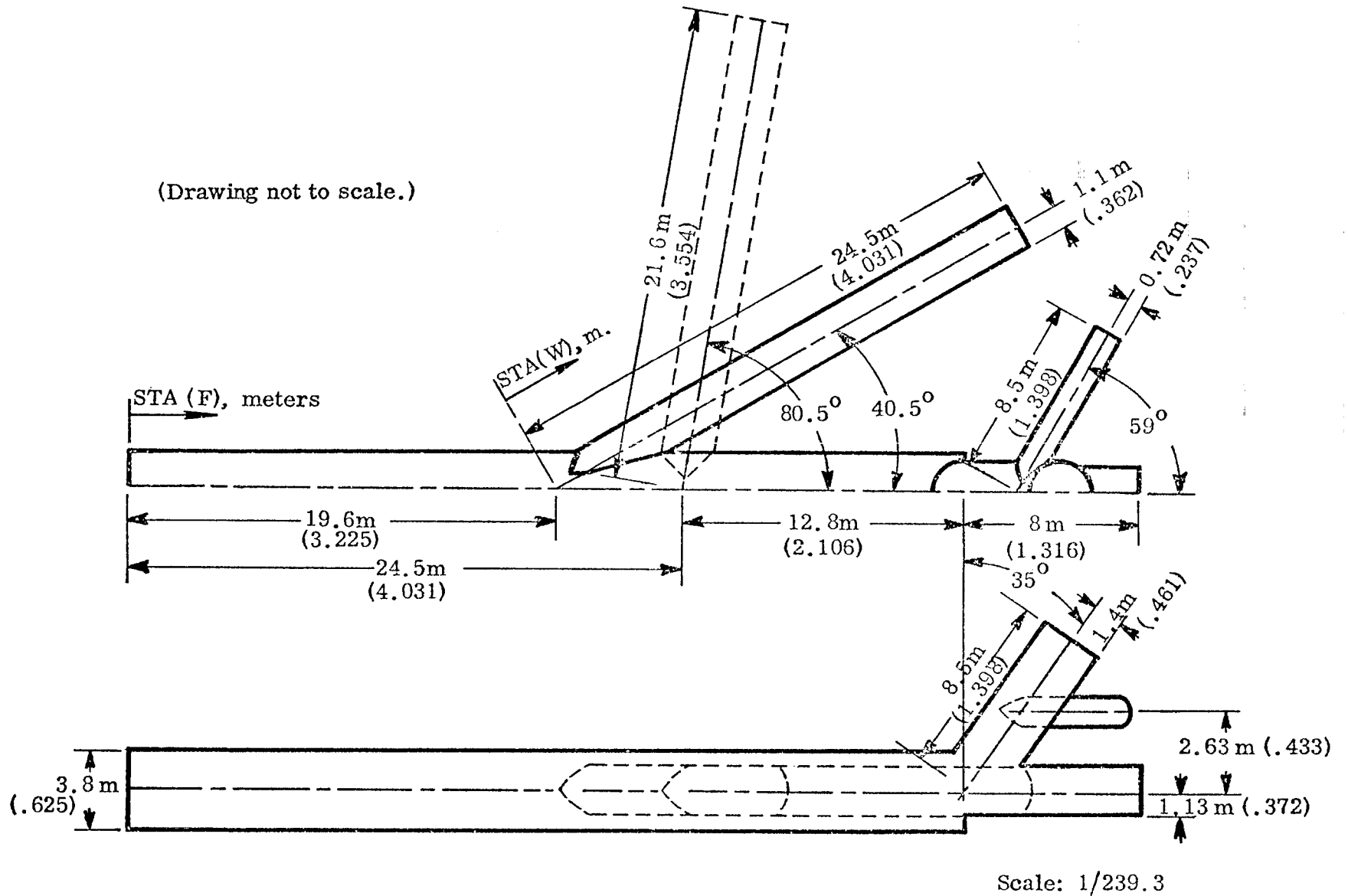
1.13 m (.372)

Scale: 1/239.3

FIG. 29: B-1 wire model used for skin current measurements. Full scale dimensions are in meters; in parentheses are model dimensions in inches.

TABLE 1

Incident polarization with respect to fuselage	Illumination	Points where measurements were made	Figures where data are presented
parallel	top	center of fuselage, top, STA = 22.65 (F)	Figs. 30, 31
parallel	top	center of fuselage bottom, STA = 22. 65 (F)	Figs. 32, 33
parallel	top	near cockpit, top, wings forward, STA = 5.0 (F) wings swept, STA = 5.55 (F)	Figs. 34, 35
perpendicular	top	center of fuselage, top, STA = 22.65 (F)	Figs. 36, 37
perpendicular	top	center of wings, top, wings forward, STA = 10.8 (W) wings swept, STA = 12.25 (W)	Figs. 38, 39

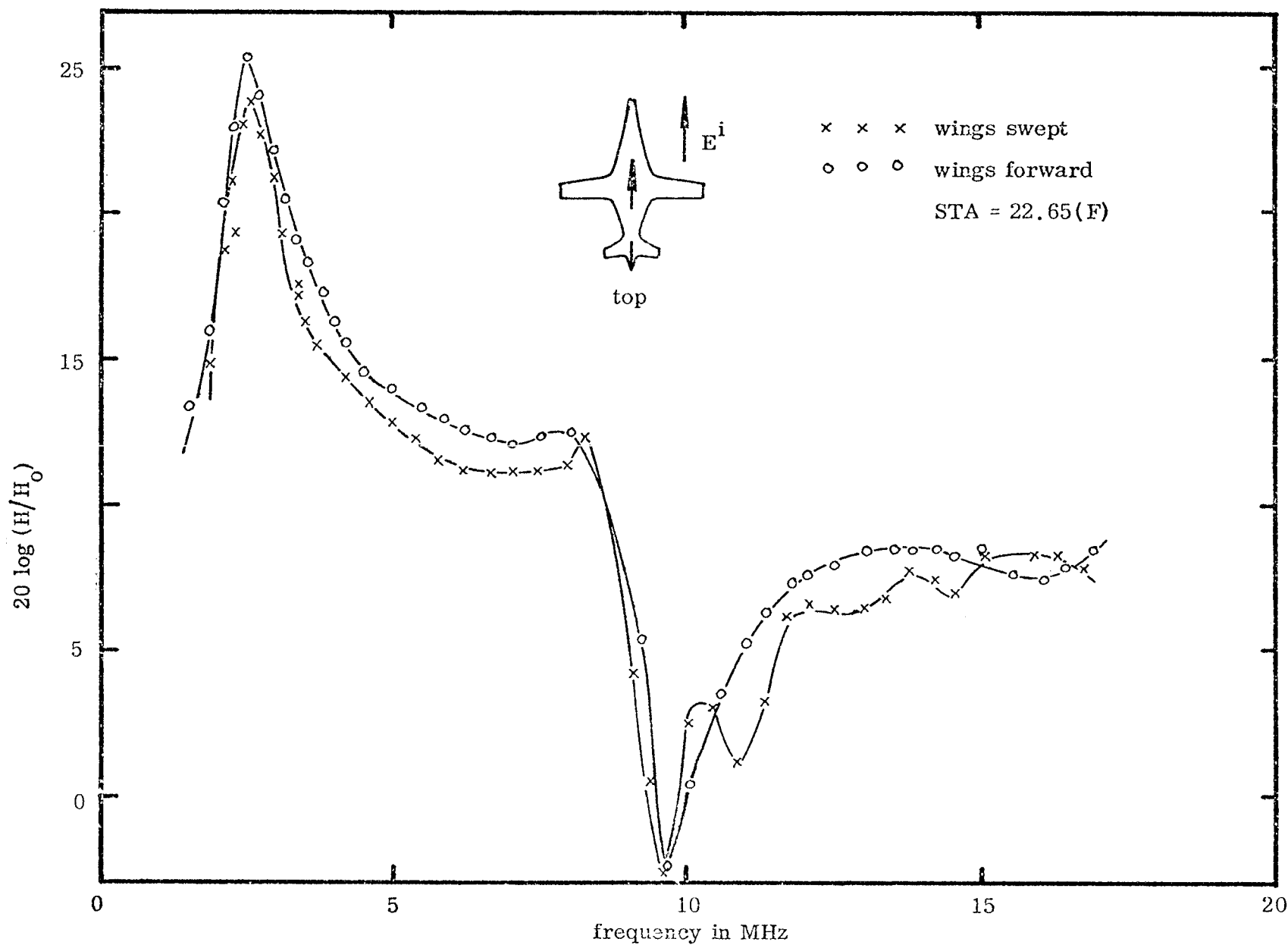Summary of measurements and data presented for the wire grid model of the B-1 aircraft.

60

FIG. 30: B-1 wire model, current amplitude on top of the fuselage at center; top illuminated, E^i parallel to fuselage.
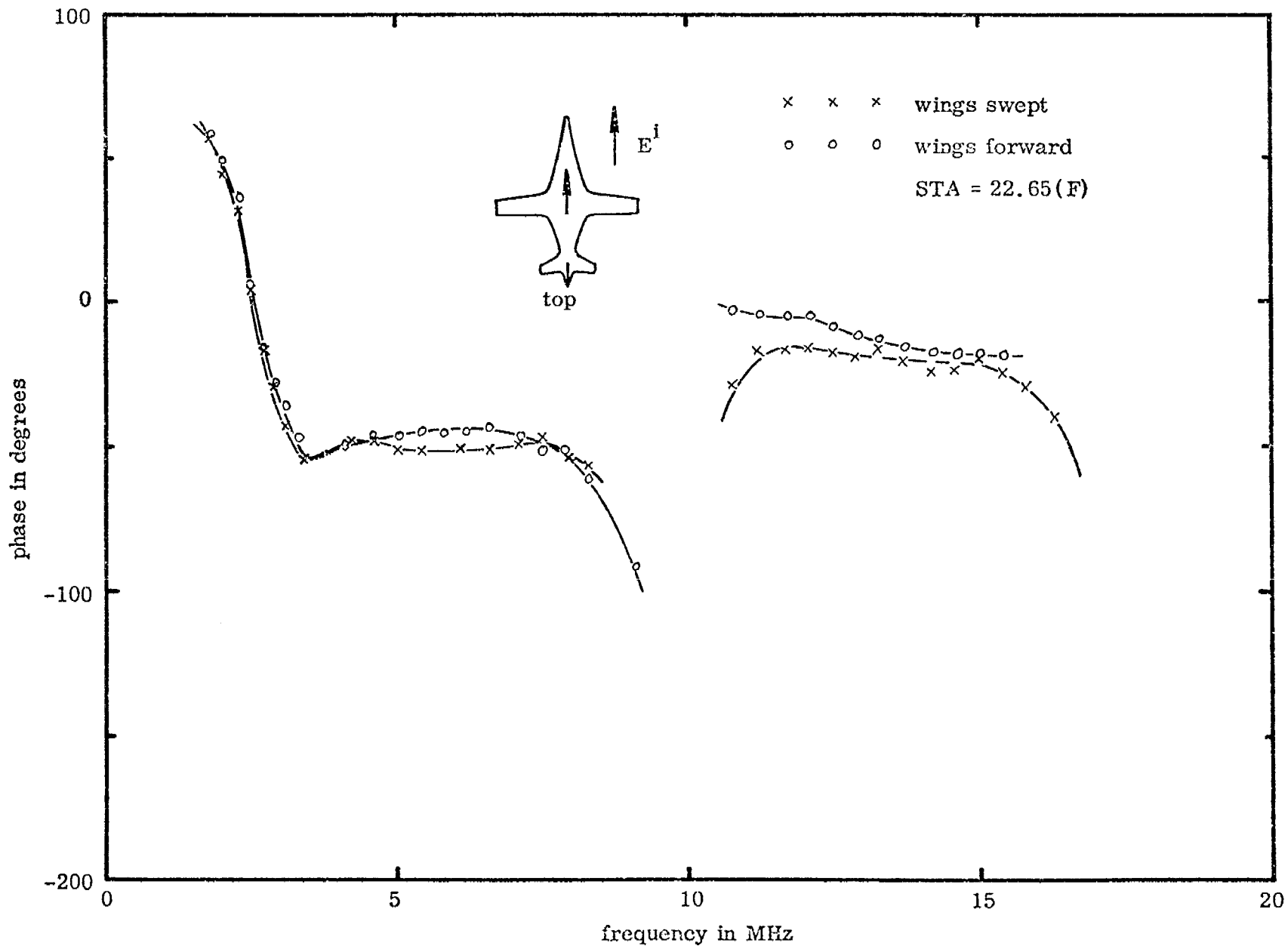
FIG. 31: B-1 wire model, phase on top of the fuselage at center; top incidence, E^i parallel to fuselage. Phase reference is top of fuselage.
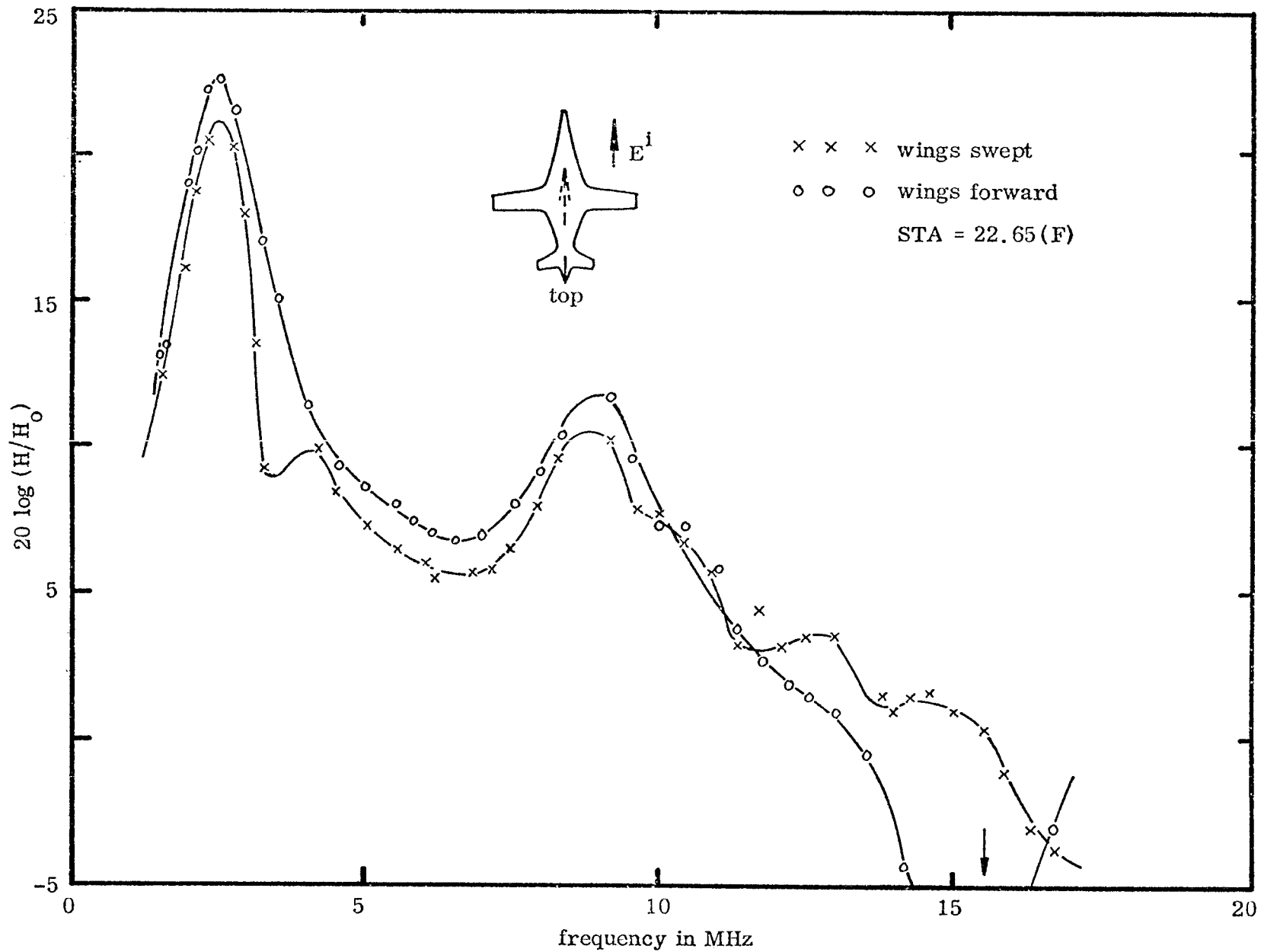
FIG. 32: B-1 wire model, current amplitude on bottom (shadow side) of the fuselage at center; top incidence, E^i parallel to fuselage.
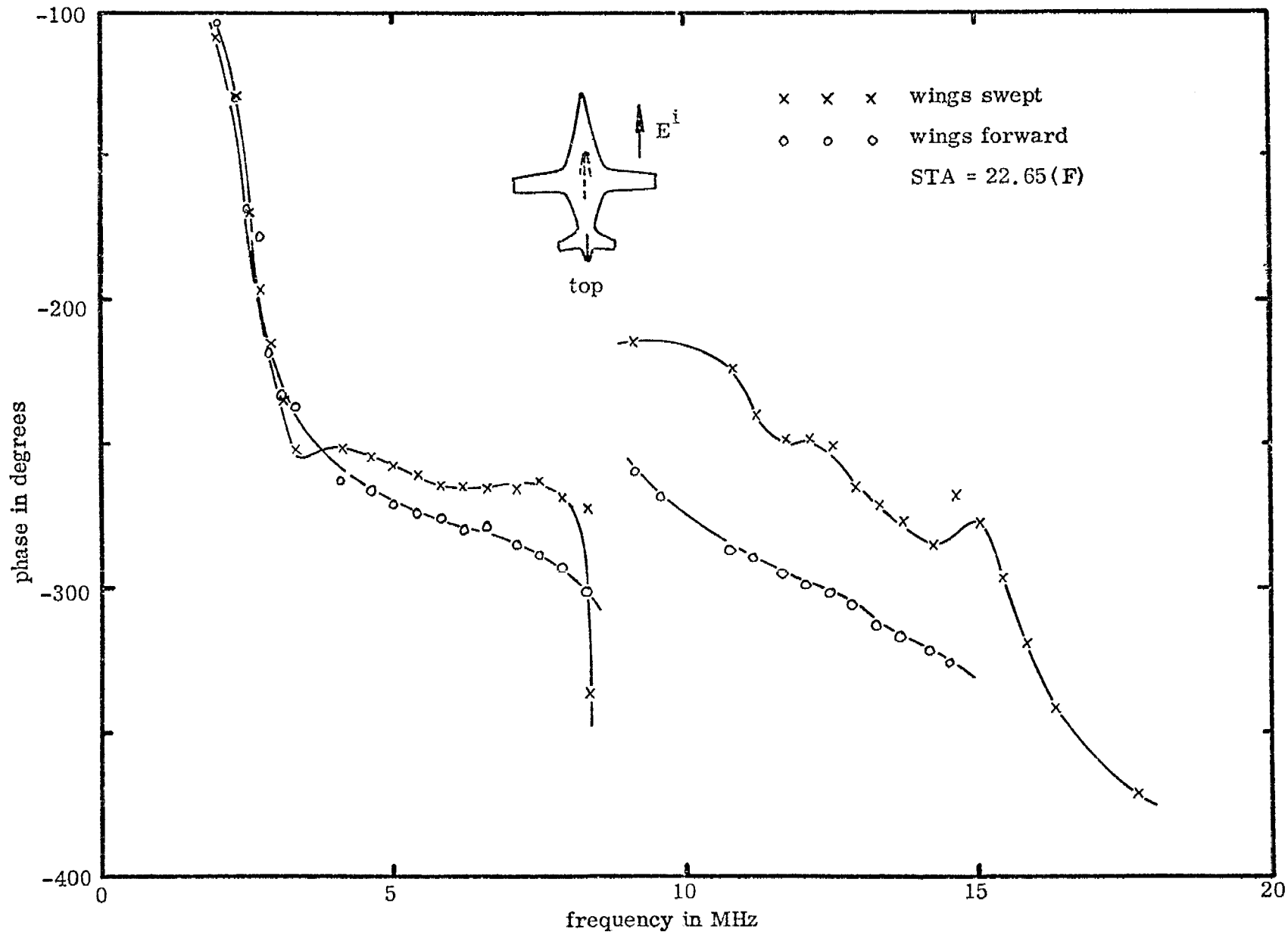
FIG. 33: B-1 wire model, phase on bottom (shadow side) of the fuselage at center; top incidence, E^i parallel to fuselage. Phase reference is top of fuselage.
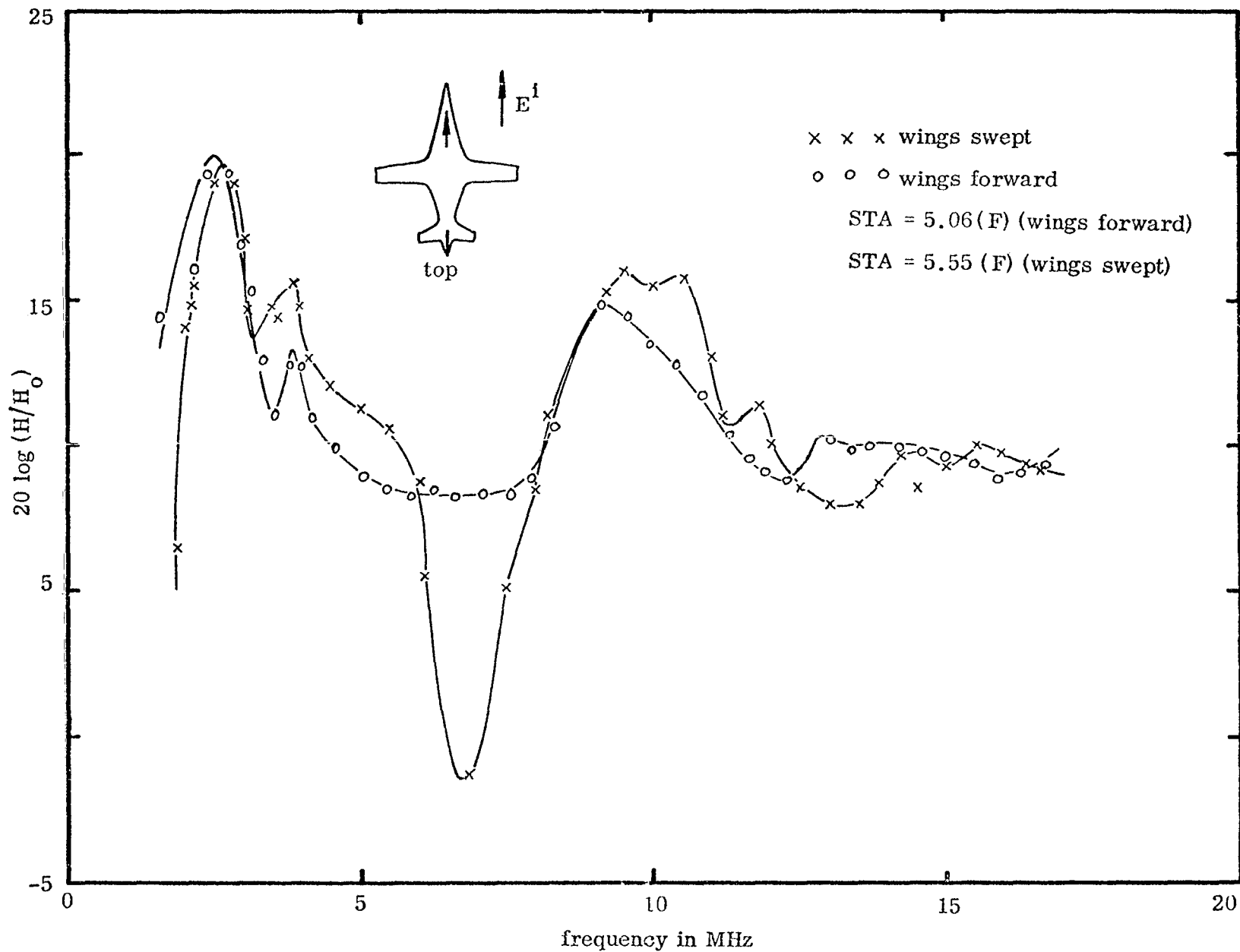
FIG. 34: B-1 wire model, current amplitude near cockpit; top incidence, E^i parallel to fuselage.

FIG. 35: B-1 wire model, phase near cockpit; top incidence, E^i parallel to fuselage. Phase reference is top of fuselage.

FIG. 36: B-1 wire model, current amplitude on top of the fuselage; top incidence, E^i perpendicular to the fuselage.

FIG. 37: B-1 wire model, phase on top of the fuselage; top incidence, E^i perpendicular to fuselage. Phase reference is top of fuselage.

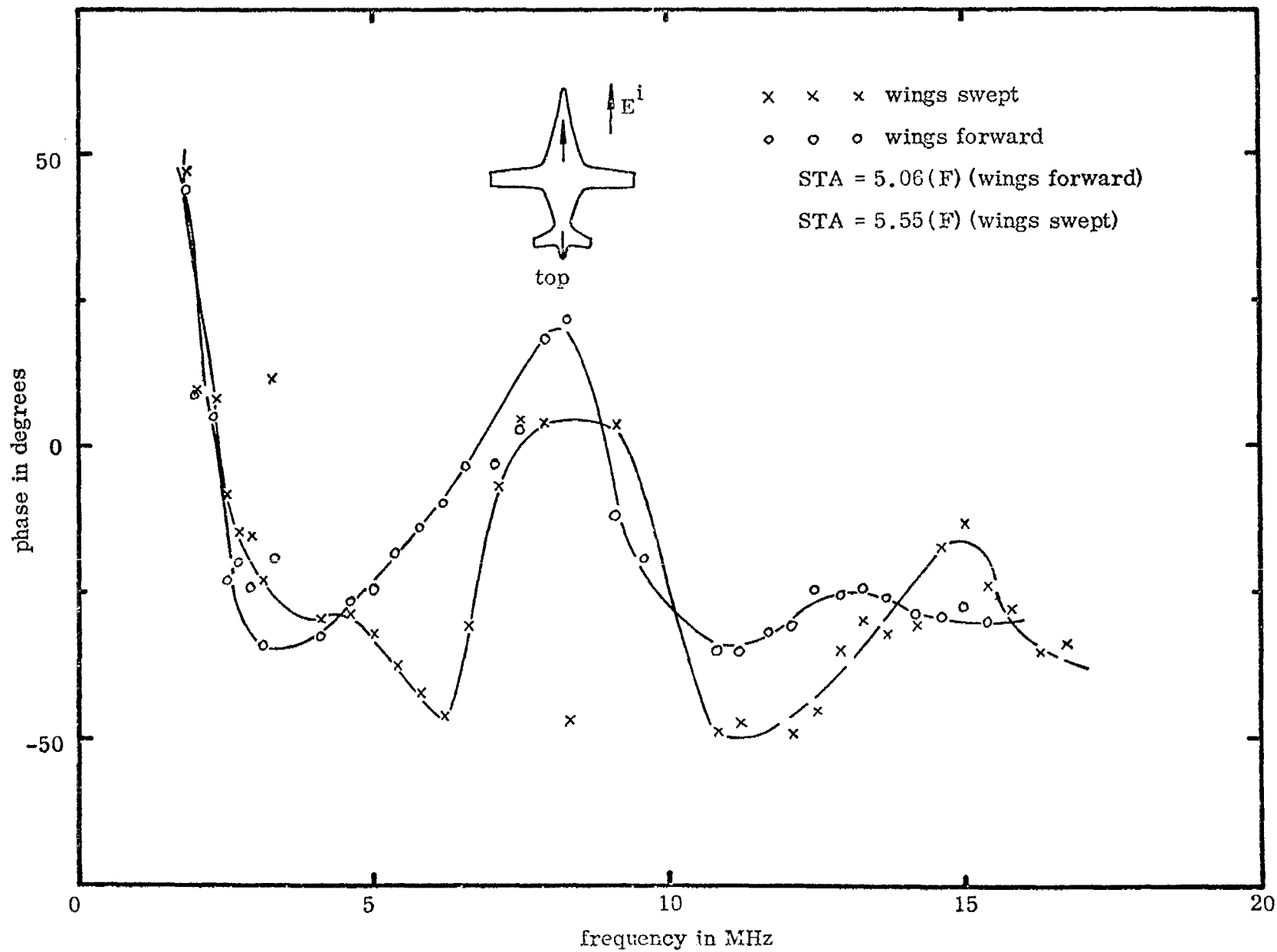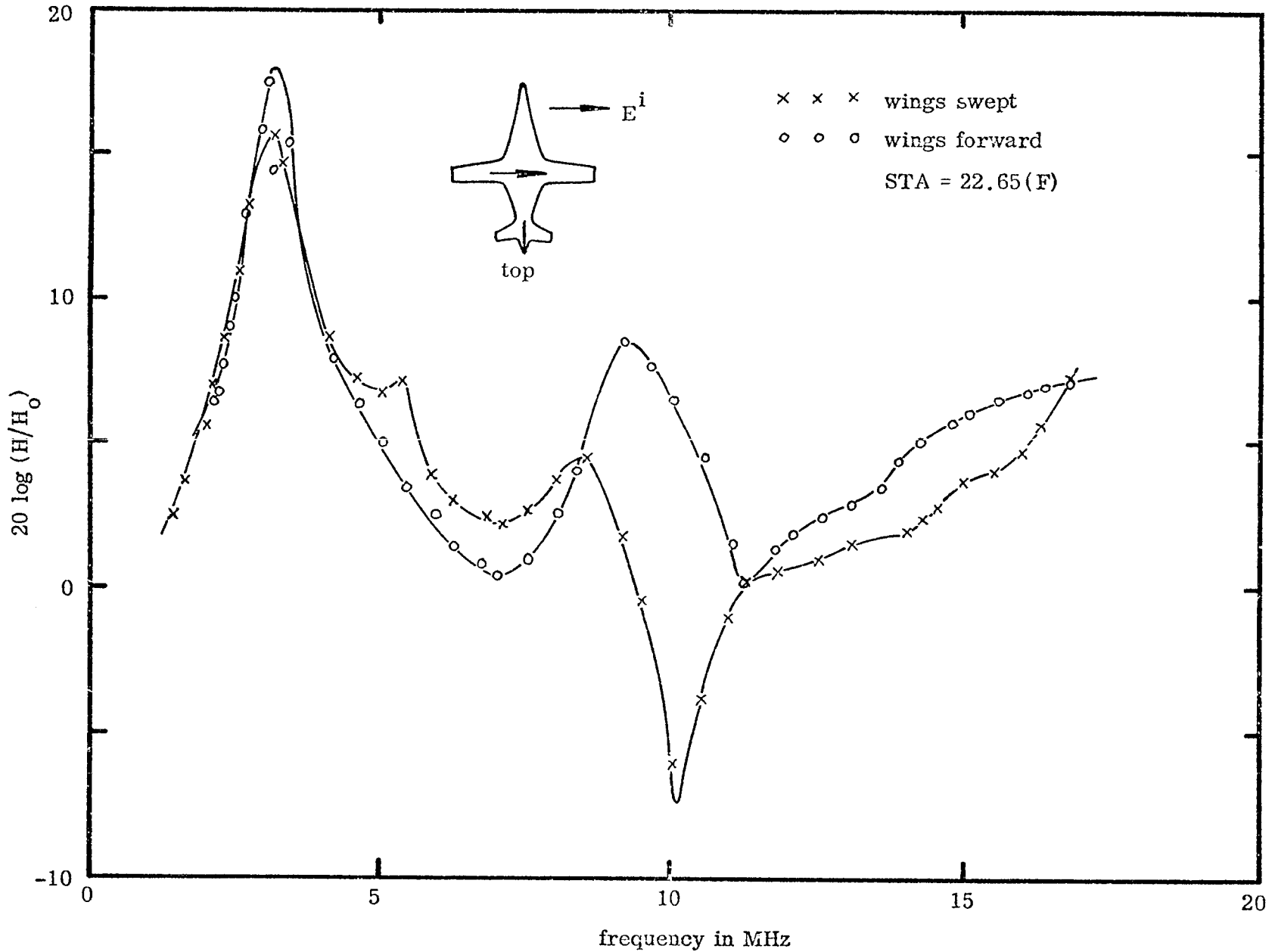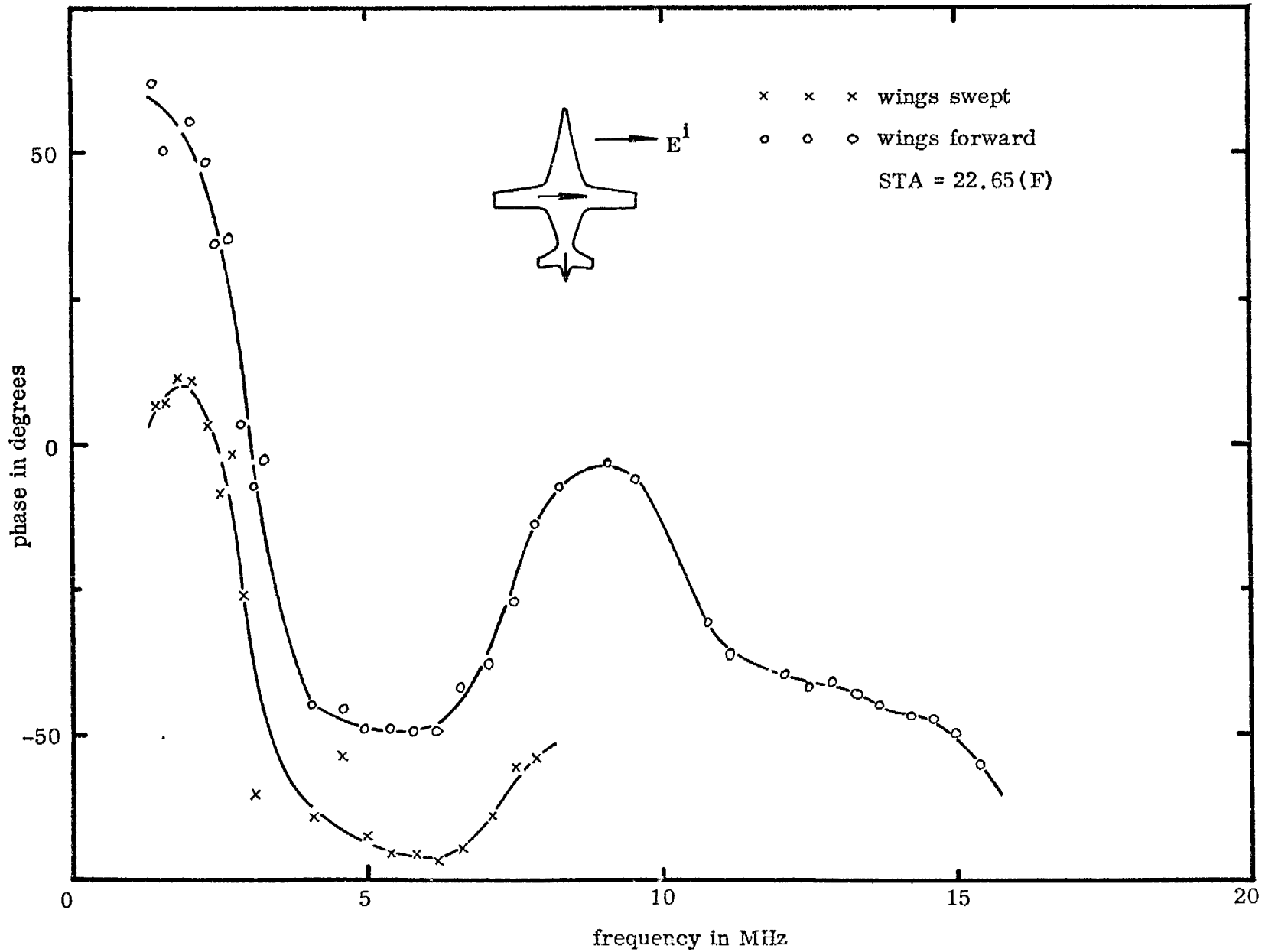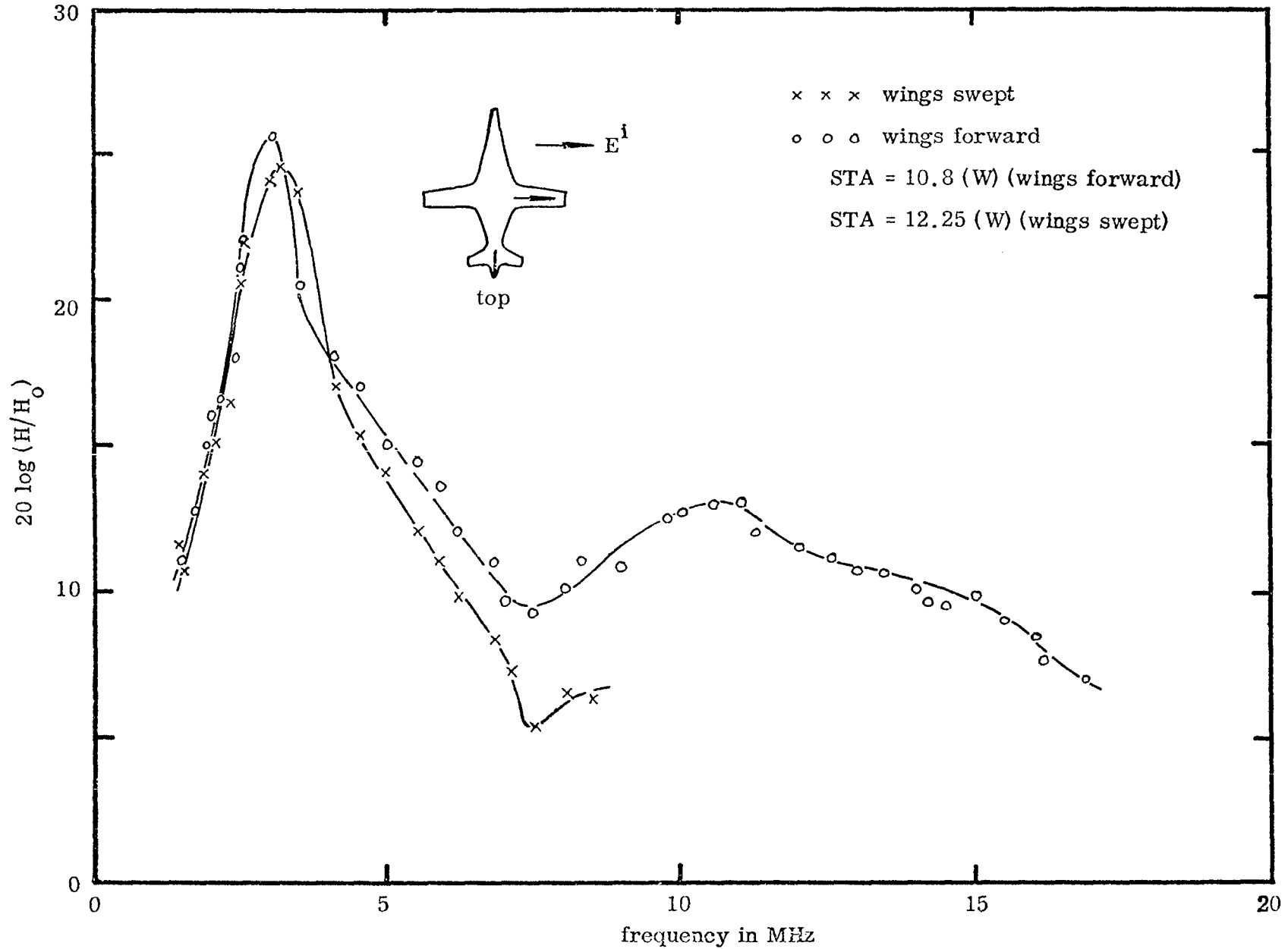FIG. 38: B-1 wire model, current amplitude on top of the wing; top incidence, E^i perpendicular to fuselage.
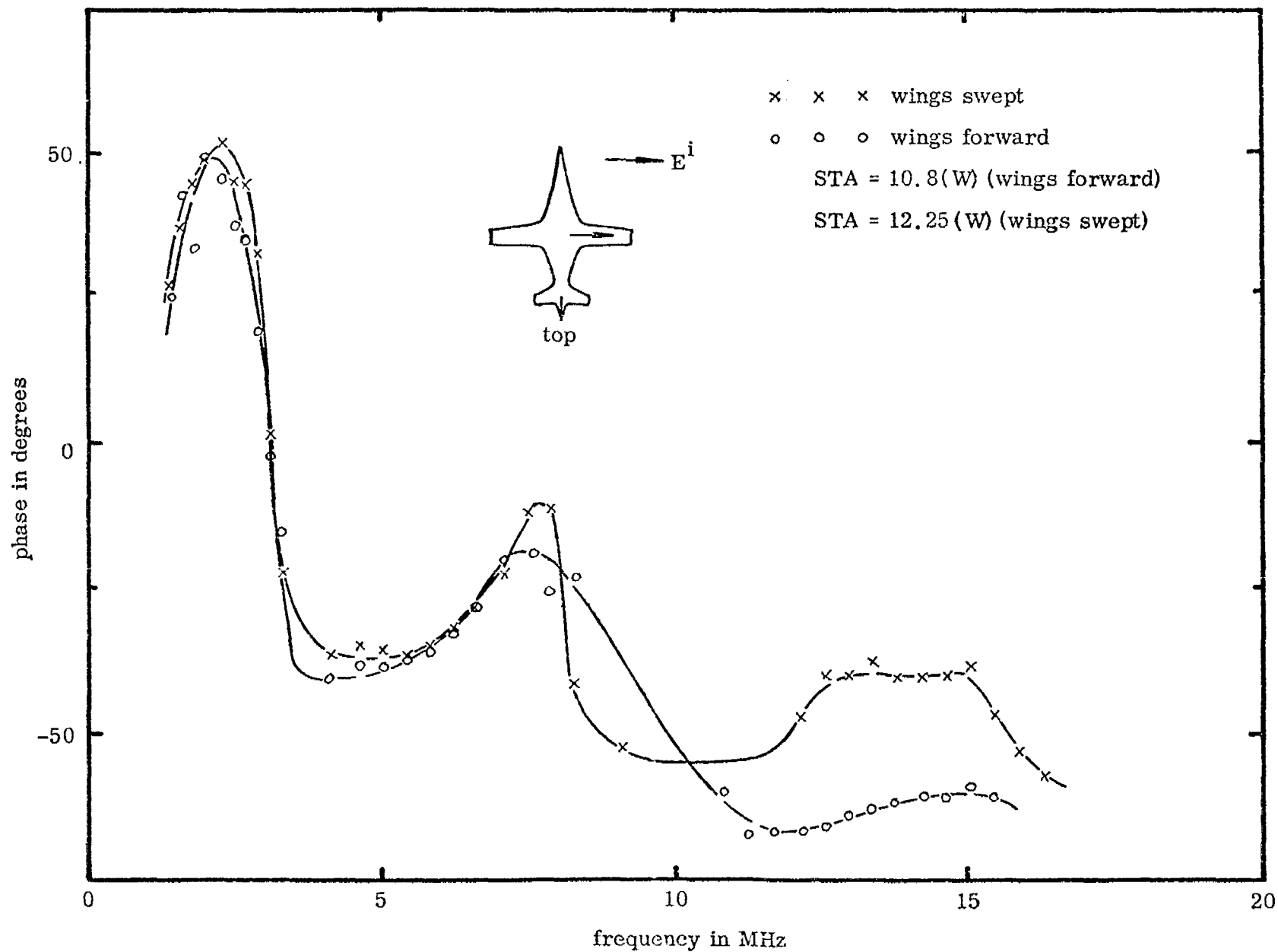
FIG. 39: B-1 wire model, phase on top of the wing; top incidence, E^i perpendicular to fuselage. Phase reference is top of fuselage.

priate to 0.362 in. wing diameter, has been added to the wing data in Fig. 38. The data for the circumferential current measured on top the fuselage (Fig. 36) has not been adjusted since the correction factor is not available.

For measurements presented in this section top incidence was always used with the incident electric vector (polarization) parallel or perpendicular to the fuselage. The phase reference was the topside of the fuselage. The measurements were made in four frequency bands, 0.35-0.8 GHz, 0.8-1.0 GHz, 1.0-2.0 GHz and 2.0-4.0 GHz; using the 1/239.3 model scaling factor the corresponding full scale frequency range is 1.47-16.7 MHz. In covering this frequency range data is not available for some frequency bands due to loss of track by the network analyzer. This occurred as a result of operating the equipment beyond its designed frequency range. In particular, this is true with the transmitting antennas. In the 2-4 GHz range, for example, a standard S-band horn antenna was used, and there a tracking drop-out was typically experienced in the 2.0-2.2 GHz range. In the 1.0-2.0 GHz band, where an L-band horn antenna was used, a drop-out occurred in the 1.8-2.0 GHz range. Likewise, for frequencies below 1.0 GHz dropouts were experienced, but in most instances these were corrected by retuning the broadband sleeved antenna used in transmitting. In data presented (Figs. 30 through 39) the dropout ranges are more predominant in the phase data. It should be noted that the lines connecting the data points are merely for showing the curve shape and their shape may be in question where large gaps in data occur.

When making a comparison of measured data and that generated by computer codes one should have a clear understanding of what the fields actually are. The measured current and charge presented here are total fields and include the incident field component. On the other hand, depending upon the formulations, the computer-generated fields may not include the incident field. For example, it appears that the fuselage current as presented by Taylor et al. (ref. 2) in their Fig. 31 is the net current induced on the fuselage and to find skin current values compatible with the measurements,

the incident field should be added to the Taylor values after they have been divided by the circumference of the fuselage. To perform such an addition, the phase of the current and of the incident field is required. Therefore, such calculation would best be performed by the computer when the currents are computed. An alternative would be to subtract the incident field from the measured data, but this procedure would be more complicated.

Because there is no computer data presently available for the particular wire grid models used in these measurements, no comparison of measured and computed data is made. However, data for the top of the fuselage (Fig. 30) and for near the cockpit (Fig. 34), computed using a 1 meter common radius for the model, is available (ref. 6). They show the same first resonant frequency and the same general shape of the current curves, but are 5 to 7 dB higher in amplitude.

6. T. L. Brown, "Application of a Wire Computer Code to the B-1 Aircraft," Interaction Application Memos, Memo 8, Air Force Weapons Laboratory, Kirtland AFB, NM, July 1975.

SECTION V

SUMMARY

A description of a surface field measurement facility that uses a sweep frequency measurement technique and records signals proportional to currents or charges as a function of frequency has been presented. Numerous supplementary studies including the design and performance of charge probes and charge probes with built-in diodes and high resistance telemetry leads are included. An investigation of the use of current loop probes for measurements along elements of small radius of curvature is described along with calibration information on these probes.

Of particular interest are the current data presented for the 747 aircraft and the wire grid model used in computation of currents on B-1 aircraft. The 747 aircraft surface current data are presented in conjunction with "rough scale" model studies in which the 747 model results are compared with the current measured on two rough models of the 747 aircraft. The study suggests that rough models can be used at the first resonance and lower frequencies for measuring the currents that would represent values for the detailed model, but certain model details must be included. For example, for antisymmetric excitation, the presence of engines does appear to lower the first resonance peak of the current excited over the wings and for such measurements the engines should be included. For measurements of fuselage current, symmetric excitation, engines have no noticeable effect; the length and diameter of the fuselage are the important dimensions. The data for the wire grid model cover the 1.5 to 16.5 MHz (full scale) frequency range and include amplitude and phase measurements for five different stations on the body. The resonances are clearly explicit and agree (in frequency) with the computed results.

The development of the current measurement facility described herein is a continuing process and techniques are updated as new techniques and instruments are developed. Judging from the data of current and charge measured on spheres, the following specifications seem appropriate for the facility.

(Scale) frequency coverage:	0.500 - 6.0 GHz
Maximum size of the model:	2 feet
Expected accuracy:	
0.5 to 1 GHz	$\pm$ 3 dB in amplitude $\pm$ 10 degrees in phase
1 to 4 GHz	$\pm$ 1 dB in amplitude $\pm$ 5 degrees in phase
4 to 6 GHz	$\pm$ 3 dB in amplitude $\pm$ 10 degrees in phase

These estimates are not final, and as techniques and equipment change accuracy improvements can be expected. For example, the frequency range of operation is presently limited at the low end by errors caused by the interaction between the model and the chamber, but the errors and the frequency range of operation can be lowered by redesigning the chamber for lower frequency operation. The operation above 6 GHz is limited as the current and charge probes become electrically "large" and consequently begin to introduce undesired averaging effects in the measurements. A continuing improvement in design and miniaturization of sensors should extend the upper frequency operating range.

The two-foot maximum size of the model is given only as a guideline and has been deduced from the $2D^2/\lambda$ far field criterion used in radar cross section back scattering measurements, where D is the maximum dimension of the object. If needed, objects as large as 5 feet could be placed inside the chamber, but one must always keep in mind that for objects of that size the incident electromagnetic wave would not be planar. The determining criterion for selection of the maximum model size is the 35-foot distance from the transmitter antenna to the model, the permissible incident wave $1/r$ amplitude decay over the model along the direction of propagation and the permissible frontal phase error due to the spherical nature of the wave.

Finally, the measurement accuracy of $\pm$ 1 dB or $\pm$ 3 dB (depending upon the frequency range considered) has been based on past measurement experience and sample data presented here. The measurement accuracy depends on many factors, some of which are the size of the model, the frequency range used, the care used in

making the measurements and the general condition of the facility and instrumentation. Probes also play an important role, especially the telemetry lead for the charge probe. Techniques of averaging the data over a number of measurements obtained after slight systematic repositioning of the model and the telemetry leads in the chamber would improve the resultant accuracy, but the task of data reduction would then become enormous. In such case, an automated data reduction scheme should be considered.

747 MEASUREMENT STATION DESIGNATION